

Topical Issue - 10 years of JSWSC

RESEARCH ARTICLE

OPEN  ACCESS

The Interplanetary and Magnetospheric causes of Geomagnetically Induced Currents (GICs) > 10 A in the Mäntsälä Finland Pipeline: 1999 through 2019

Bruce T. Tsurutani^{1,*} and Rajkumar Hajra²

¹ Jet Propulsion Laboratory, California Institute of Technology, Pasadena, California 91109, USA

² Indian Institute of Technology Indore, Simrol, Indore 453552, India

Received 9 October 2020 / Accepted 7 January 2021

Abstract—The interplanetary and magnetospheric phenomena time-coincident with intense geomagnetically induced current ($GIC > 10 A$ and $> 30 A$) events during 21 years (1999 through 2019) at the Mäntsälä, Finland (57.9° magnetic latitude) gas pipeline have been studied. Although forward shocks and substorms are predominant causes of intense GICs, some newly discovered geoeffective interplanetary features are: solar wind plasma parcel (PP) impingements, possible interplanetary magnetic field (IMF) northward (B_n) and southward (B_s) turnings, and reverse shocks. The PPs are possibly the loop and filament portions of coronal mass ejections (CMEs).

From a study of $> 30 A$ GIC events, it is found that supersubstorm ($SSS: SML < -2500 \text{ nT}$) and intense substorm ($-2500 \text{ nT} < SML < -2000 \text{ nT}$) auroral electrojet intensifications are the most frequent (76%) cause of all of these GIC events. These events occur most often (76%) in superstorm ($SYM-H \leq -250 \text{ nT}$) main phases, but they can occur in other storm phases and lesser intensity storms as well. After substorms, PPs were the most frequent causes of Mäntsälä $GIC > 30 A$ events. Forward shocks were the third most frequent cause of the $> 30 A$ events. Shock-related GICs were observed to occur at all local times.

The two “Halloween” superstorms of 29–30 and 30–31 October 2003 produced by far the greatest number of GICs in the interval of study (9 $> 30 A$ GICs and 168 $> 10 A$ GICs). In the first Halloween superstorm, a shock-triggered SSS ($SML < -3548 \text{ nT}$) caused 33, 57, 51 and 52 A GICs. The 57 A GIC was the most intense event of the superstorm and of this study. It is possible that this SSS is a new form of substorm. Equally intense magnetic storms were also studied but their related GICs were far less numerous and less intense.

Keywords: GIC / Supersubstorm / Plasma Parcel / Shock / ICME / Superstorm

1 Introduction

Geomagnetically induced currents (GICs) are currents induced in the solid Earth or in conductors on the Earth's surface by sudden, intense currents flowing in space plasmas. Such a phenomenon was noted a century and a half ago when the deflection of telegraph magnetic needles of the Midland Railroad (England) was observed to be coincident with auroral sightings (Barlow, 1849). Currents were noted to flow even when the batteries were not connected. More recently Campbell (1980) observed electric currents flowing in the Alaska oil pipeline and deduced that the source was the auroral electrojet

current (a midnight sector current flowing in the ionosphere at $\sim 100 \text{ km}$ altitude with intensities of up to and possibly greater than 10^6 A).

This paper was motivated by the extensive GIC data set existing for the natural gas pipeline near Mäntsälä, Finland (57.9°N geomagnetic latitude; 60.6°N geographic latitude, 25.2°E geographic longitude; Pirjola & Lehtinen, 1985; Pulkkinen et al., 2001; Viljanen et al., 2006). Viljanen et al. (2010) performed a nice 11-year study on this data set for $GIC > 5 \text{ A}$ events during magnetic storm intervals. The purpose of this present paper is to identify for the first time the interplanetary, magnetospheric and ionospheric phenomena time-coincident with intense

*Corresponding author: bruce.tsurutani@gmail.com



Special Issue – 10 years of JSWSC

> 10 A and > 30 A Mäntsälä GIC events over a 21-year interval, from 1 January 1999 to 31 December 2019.

This paper is intended to be a top-level survey, to identify the possible relationship between Mäntsälä intense GIC events and interplanetary time-coincident features. We will also identify the Mäntsälä GIC relationships with magnetic storms and substorms (which are causes by interplanetary magnetic field (IMF) southward component B_s) to obtain information about the relationship between the intensity of the GICs and the intensities of the magnetospheric and ionospheric activity.

We caution the reader that Mäntsälä is located at subauroral (57.9° magnetic) latitudes, so the interplanetary and magnetospheric causes of GICs at auroral latitudes, mid-latitudes, and equatorial latitudes might be different. Similar studies on other data sets will be needed to determine the causes of GICs at these other regions of the Earth.

Why are we performing this study? All GIC events on Earth are believed to be ultimately related to interplanetary drivers. The dB/dt events that cause Mäntsälä GICs could also cause GICs in other subauroral systems. Of course, the GIC intensities for the other subauroral systems will be different (owing to different physical layouts, ground conductances, etc.), but statistically the physical interplanetary causes may be the same. A survey of this type has never been performed before. It will be shown that new, important potential causes of GICs at Mäntsälä will be discovered.

2 Databases, methods of analyses, and related background space plasma observations

2.1 GIC data

This study was undertaken using the current intensity measurements taken from the natural gas pipeline near Mäntsälä, Finland (57.9°N geomagnetic). See Pulkkinen et al. (2001) and Viljanen et al. (2010) for more details. Viljanen et al. (2010) have indicated that the Mäntsälä GIC measurement noise level is about 1 A. The measurements were taken at 10 s intervals and for this study, we examine only the largest events with intensities of 10 A (and also 30 A) current or greater. The study covers an interval of time from 1 January 1999 to 30 December 2019, almost two full solar cycles. Event intervals with GICs larger than 10 A (and 30 A) are recorded and are discussed in the Appendix. All of the GIC event data have interplanetary and geomagnetic activity data superposed, and are shown as figures in the Appendix. The GIC data are available from the Space and Earth Observation Centre of the Finnish Meteorological Institute (<https://space.fmi.fi/gic/index.php>). The solar wind and geomagnetic activity data are discussed separately, below.

Figure 1 shows the Mäntsälä GIC data availability over the study interval as a function of solar activity cycle phase. The top panel is the solar F10.7 radiation intensity in solar flux units (sfu) as a function of year (bottom panel, horizontal axis), indicating the phase of the solar cycle. 1999 is in the ascending phase of solar cycle 23 (SC23) and 2019 is in the minimum phase between SC24 and SC25. The bottom panel shows the Mäntsälä data availability with the universal time (UT) given as the vertical axis. Smoothing was performed to give a general indication for

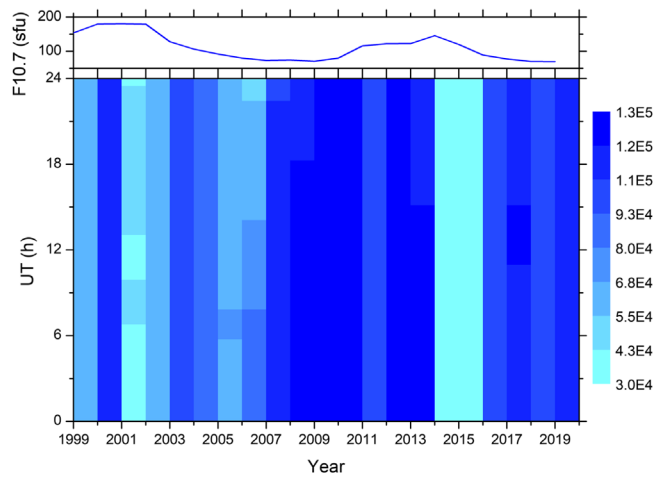


Fig. 1. The GIC data coverage for this study. The top panel gives the F10.7 solar flux in solar flux unit (sfu), where a sfu is $10^{-22} \text{ W m}^{-2} \text{ Hz}^{-1}$. The bottom panel gives the universal time (UT) of Mäntsälä in the vertical axis and year in the horizontal axis. The legend for the lower panel color figure on the right shows the numbers of 10 s GIC observations during each UT-year sector.

the reader. The legend is given on the right. It can be noticed that during the year 2014–2015 where the coverage was “low”, there were still over 30,000 10 s GIC data intervals available. The top coverage occurred between 2007–2013 and 2016–2019 with over 100,000 10 s intervals at all UTs. The difference between year 2014 and 2015 and the maximum coverage is only a factor of 3 times. We conclude that the GIC data coverage at Mäntsälä over the interval of study was quite good.

For our study, Mäntsälä GIC data was available for 128,506 h out of 184,080 h possible (21 years), or 69.8% of the time. We have used cutoff intensities of > 10 A and > 30 A for this present study. There were 605 > 10 A and 21 > 30 A GIC events found in this study.

The Mäntsälä GICs were noted to develop with time. GIC events could be as short as 20 s and as long as 13 min. The average duration was ~2 min. In this paper we plot the event at the time of the peak intensity, rounded to the nearest minute.

2.2 Solar wind data

The solar wind and IMF data (1 min time resolution) were obtained from the OMNI website (<https://omniweb.gsfc.nasa.gov/>). The solar wind data for the 29–30 October and 30–31 October 2003 “Halloween storms” were obtained from R. Skoug and were used in the Mannucci et al. (2005) paper. The magnetic field components are given in geocentric solar magnetospheric (GSM) coordinates.

2.3 Geomagnetic activity data: magnetic storms

The geomagnetic $SYM-H$ and Dst indices were obtained from the World Data Center for Geomagnetism, Kyoto, Japan (<http://wdc.kugi.kyoto-u.ac.jp/>). The 1 min average $SYM-H$ indices and the 1 h Dst indices will be used to identify magnetic storm occurrences and intensities.

Magnetic storms are identified by the criteria $SYM-H \leq -50 \text{ nT}$ (Gonzalez et al., 1994). For each magnetic storm that occurred related to Mäntsälä GIC events > 10 A, the peak storm

intensity (to the nearest nT) will be given. In addition, we will identify superstorms with $SYM-H \leq -250$ nT (Tsurutani et al., 1992; Gonzalez et al., 2007; Echer et al., 2008a; Meng et al., 2019) to indicate a higher-level cutoff of storm intensity. Superstorms will be shown to play a major role with the production of GICs.

The causes of magnetic storms have been well established to be due to the process of magnetic reconnection between southward IMFs (Bs) and the northward magnetic fields of the Earth's dayside magnetopause (Dungey, 1961) and the formation of a magnetospheric ring current (Williams, 1985; Daglis et al., 1999). This relationship between the IMF Bs and magnetic storms has been well documented in the literature (e.g., Gonzalez & Tsurutani, 1987; Tsurutani et al., 1988; Gonzalez et al., 1989, 2007; Zhang et al., 2007; Echer et al., 2008b; Meng et al., 2019) and will be noted in the examination of magnetic storm events.

IMF northward (Bn) turnings cause cessation of ongoing geomagnetic activity and lead to geomagnetic quiet conditions (Tsurutani & Gonzalez, 1995; Du et al., 2008). Several of the latter cases will be noted in the results of this paper.

2.4 Geomagnetic activity data: substorms

The geomagnetic *AL* and *AU* indices were obtained from the World Data Center for Geomagnetism, Kyoto, Japan (<http://wdc.kugi.kyoto-u.ac.jp/>). The 1 min average, ~12 station *AL* and *AU* indices are located near the auroral oval and are best used to identify substorms during relatively low to moderate level geomagnetic activity.

The 1 min average *SML* and *SMU* indices were taken from the SuperMAG network (<http://supermag.jhuapl.edu/>). These indices are based on ~300 ground-based magnetometers and give much finer spatial scale resolution plus subauroral latitudinal coverage. The *SML* and *SMU* indices are particularly useful during magnetic storms when auroras occur at locations below the auroral oval (at midlatitudes).

In this paper the peak *SML* intensity of pertinent substorms will be noted. In addition, substorms will be sorted into regular “substorms” (-50 nT $>$ *SML* $>$ -2000 nT), “large substorms” (-2000 nT $>$ *SML* $>$ -2500 nT) and “supersubstorms” (SSSs: *SML* $<$ -2500 nT, Tsurutani et al., 2015) to give a general sorting of substorm intensities.

Isolated substorms, those that occur outside of magnetic storms have been shown to be caused by IMF Bs intervals (Tsurutani & Meng, 1972; Meng et al., 1973). The IMF Bs turnings led to substorm onsets and subsequent IMF Bn turnings led to substorm terminations. What is the difference between IMF Bs for substorms and the much larger magnetic storms? The IMF Bs for isolated substorms were of a shorter-duration (~30 min to ~1 h compared to ~1 h to ~3 h) and of lower intensities (~5 to ~10 nT in comparison to ~20 to ~100 nT).

2.5 Interplanetary shocks

Interplanetary fast forward shocks (“shocks”) will be identified by their abrupt increases in solar wind velocity (V_{sw}), density (N_{sw}), temperature (T_{sw}), and IMF magnitude (B_0). Interplanetary fast reverse shocks are noted by their abrupt increases in V_{sw} and simultaneous decreases in N_{sw} , T_{sw} and B_0 (Kennel et al., 1985; Stone & Tsurutani, 1985; Tsurutani & Stone, 1985; Tsurutani et al., 2011). To identify the properties

of the shocks (quasi-parallel: Kennel et al., 1984a, b or quasi-perpendicular, Mach number, ram pressure), detailed high resolution upstream and downstream plasma and magnetic field properties must be used to identify the shock normal direction relative to the upstream magnetic field and the Rankine-Hugoniot relations to obtain the shock Mach number. These detailed calculations will be foregone for the present. In this study we will tentatively identify shocks by their jump conditions alone. A more detailed study of shocks and their GIC effects will be postponed for a second, follow-up study. Why is it necessary to eventually identify shocks using the Rankine-Hugoniot conservation equations? One objective is to separate shocks from other features such as waves and tangential discontinuities (TDs). Possible density changes across TDs or compressive waves can also produce magnetospheric compressions or rarefactions.

Compression of the magnetosphere/magnetotail by interplanetary shocks can cause the triggering of substorms in the nightside magnetosphere. These triggered substorms can be particularly intense (Hajra & Tsurutani, 2018). For this reason, in the text that follows and in the Appendix, we have given the UT of the shocks. The local time (LT) of Finland is UT + 3 h. Thus, one can determine the LT of Mäntsälä when the shock impingement occurred on the magnetosphere. At this time we do not know whether the shock created the GIC or whether the sharp onset of the substorm triggered by the shock caused the GIC. This topic is delayed for a future study.

2.6 Interplanetary PPs (High-Plasma Densities: ICME loops? and filaments?)

Interplanetary high plasma density features of the plasma parcels (PPs) impacting the magnetosphere/magnetotail will have the same effect as interplanetary shocks. They will compress the magnetosphere and magnetotail.

2.7 Interplanetary sheaths

The sheath upstream of an interplanetary coronal mass ejection (ICME) is composed of slow solar wind plasma and magnetic fields that have been compressed, heated and swept up by the shock (Tsurutani et al., 1988). This sheath plasma and magnetic fields are therefore totally different than the ICME plasma and magnetic fields. The sheath will be referred to separately in this paper. We have also identified geoeffective solar wind events that do not have shocks. We have called these upstream regions “pileup” events without examining them in further detail here.

2.8 CMEs and their parts (loops, MCs and filaments)

A CME at the Sun has three parts: a bright outer loop, a dark region and a filament (Illing & Hundhausen, 1986; Chen, 2011). We distinguish interplanetary CMEs (ICMEs) from solar CMEs because not all three parts of a solar CME reach the Earth. In this study we have identified primarily ICME magnetic clouds (MCs; Burlaga et al., 1981) as being geoeffective and causing magnetic storms. Farrugia et al. (1997) and Tsurutani & Gonzalez (1997) have argued that the MC portion of an ICME is the dark region of a CME detected near the Sun. In this study we use the criterion of low plasma β (the ratio of the plasma thermal pressure to the magnetic pressure) to identify MCs.

Another feature of ICMEs at 1 AU are high density loops and filaments. The bright outer loop plasma and magnetic field data were identified at 1 AU by Tsurutani & Gonzalez (1995) and Tsurutani et al. (1998a). ICME filament high plasma densities were first identified in interplanetary data at 1 AU by Burlaga et al. (1998). It is possible that the high-density PPs identified in this study causing GICs are loops and filaments.

3 Results

Figure 2 shows the solar wind parameters, IMF and geomagnetic activity indices in the top 11 panels. The Mäntsälä GIC data is shown in the bottom panel. The parameters given in the various panels are identified in the figure caption. There is a shock at \sim 0612 UT on day 302 indicated by the vertical black dashed line.

The *SYM-H* index shows that this was a double dip main phase superstorm with a peak intensity of -390 nT at \sim 0148 UT on day 303. The partial cause of the first dip in the magnetic storm was the negative B_z (IMF B_s) just prior to and just after the shock (see blue trace). That and the energetic plasma injection due to the SSS (note the intense negative *SML* and *AL* at the shock; to be discussed below) triggered by the shock caused the first dip storm. This magnetic storm (and the SSS) occurred during the interplanetary sheath region of the event, from the shock at \sim 0612 UT until \sim 0938 UT. After the termination of the sheath, a MC follows. The MC ends at \sim 0244 UT on day 303. The MC B_z component is first positive (IMF B_n) and then negative (IMF B_s), consistent with a giant magnetic flux rope (Burlaga et al., 1981). The IMF B_s of the MC starts at \sim 1436 UT on day 302 and ends at \sim 0210 UT on day 303. The IMF B_s causes the second and major dip of the magnetic storm.

The shock occurred at the same time as a GIC peak of 25 A. Mäntsälä was at \sim 0912 LT (morning sector) at the time of the event. The shock also triggered a sharp onset of a two-peak SSS that lasted from \sim 0613 UT to \sim 0752 UT. The two peaks had intensities of *SML* = -3177 nT at 0624 UT and -3548 nT at 0648 UT, respectively. Associated with the first SSS were 4 GICs of intensities > 30 A. The 30 A level is indicated by a horizontal red line. The GIC intensities and times were: 33 A at 0646 UT, 57 A at 0657 UT, 51 A at 0703 UT and 52 A at 0727 UT. The SSS peaks occurred when *SYM-H* was $+13$ nT (the *SYM-H* index was not pressure corrected).

Note that enhanced GIC activity (< 10 A) is present throughout the entire \sim 21 h of the superstorm. Strong GIC activity extends from the beginning of the storm main phase to the start of the storm recovery phase. There are 168 GIC events with intensities > 10 A in the two main phases of this double dip storm. However, the most intense GIC events occurred in the first SSS immediately after the shock.

We point out several more GICs with intensities > 30 A. There is a GIC of 30 A at 2230 UT (0130 LT) near the maximum of the second dip of the superstorm. This GIC is associated with an intense substorm of *SML* = -2340 nT. There is a 36 A GIC at 0110 UT (0410 LT) on day 303 at the start of the second dip storm recovery phase. There is no obvious substorm relationship for that event.

The 29–30 October 2003 Halloween superstorm had the greatest number of GICs > 10 A (168) in the 21-year data

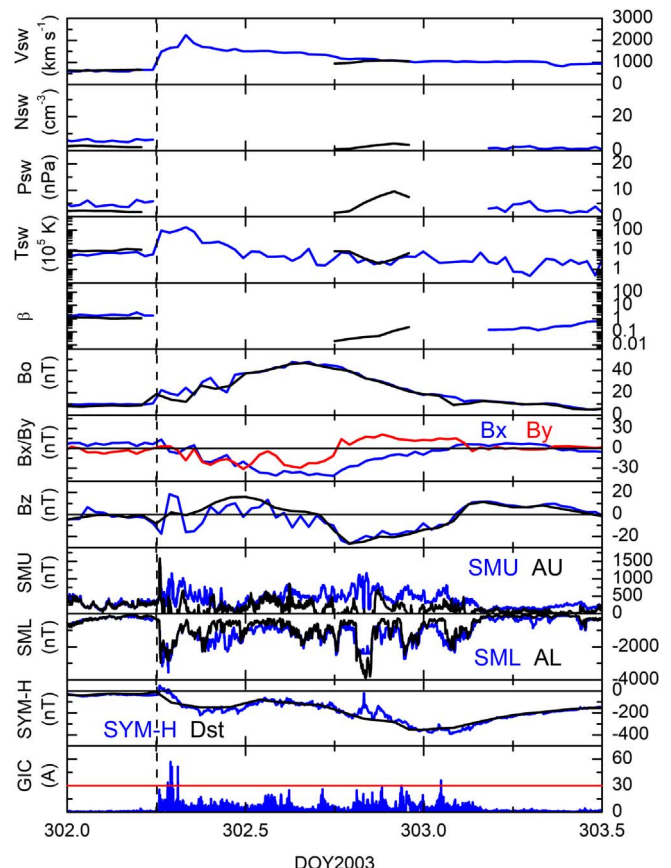


Fig. 2. The first “Halloween storm”, days 302–303 (29–30 October), 2003. From the top panel downward are the solar wind velocity (V_{sw}), density (N_{sw}), ram pressure (P_{sw}), temperature (T_{sw}), plasma β , magnetic field magnitude (B_0), the B_x and B_y components (in the same panel) and B_z in GSM coordinates. The bottom four panels are the *SMU* and *AU* indices (in the same panel), the *SML* and *AL* indices (in the same panel) and the *SYM-H* and *Dst* indices (in the same panel) and the GIC intensities. In the solar wind/interplanetary and geomagnetic indices panels, blue and black curves show 1 min and 1 h resolution data, respectively. The x -axis shows UT in the unit of day of year (DOY). The horizontal red line in the GIC panel indicates the $GIC = 30$ A intensity level. A vertical black dashed line indicates the time of an interplanetary shock.

study. These two days of a superstorm also had the greatest number of GICs > 30 A (6) in the study. The 57 A GIC at 0657 UT on day 302 was the most intense GIC detected in this study.

Figure 3 shows the second Halloween magnetic storm on days 303–304 of year 2003. A sheath B_s upstream of an ICME causes a superstorm of intensity *SYM-H* = -432 nT. A solar wind density spike (PP) at \sim 1949 UT (2249 LT) caused a SI^+ of 61 nT and triggered a short duration SSS of *SML* = -3872 nT. A GIC of 49 A occurred at the time of the shock/SSS onset.

A second short duration *SML* = -2724 nT SSS occurred in the storm main phase. It is associated with a double GIC event with peaks of 33 A and 27 A. There are two clusters of GICs with > 10 A intensities in the storm recovery phase. They are associated with substorm intervals of peak *SML* intensities of -1821 nT and -797 nT, respectively. In the first cluster there is a GIC of 30 A at 0213 UT on day 304. In the second cluster

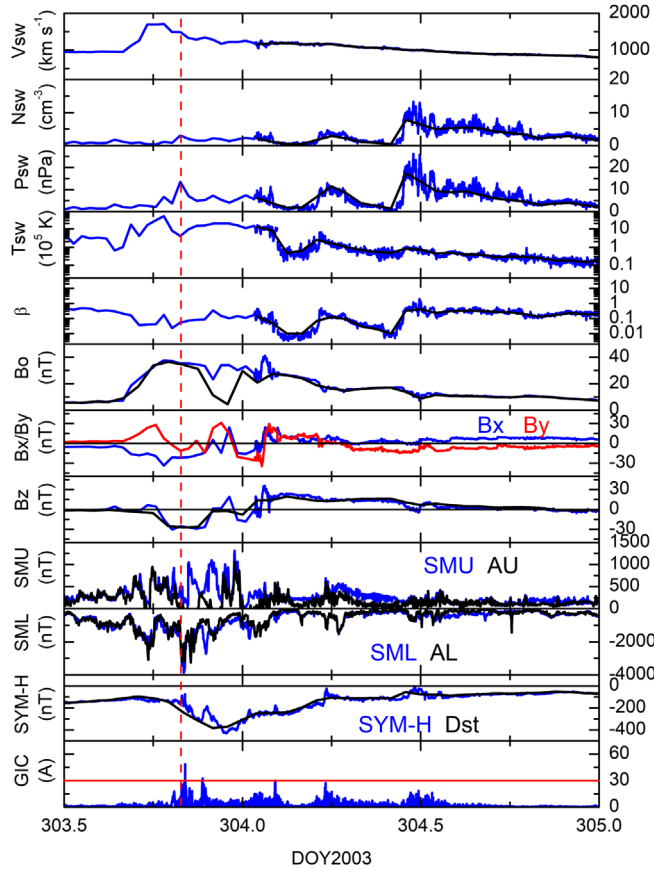


Fig. 3. Same format as in [Figure 2](#), but for the magnetic storm on days 303–304 (30–31 October), 2003. This is the second Halloween magnetic storm. The vertical red dashed line indicates a density spike (PP) incidence.

there is a 27 A GIC at 0536 UT on day 304. There is another GIC cluster, well after storm recovery, with 16 A at 1119 UT, 19 A at 1152 UT, 14 A at 1227 UT and 16 A at 1246 UT on day 304.

There were 90 GICs with > 10 A intensities on day 304. There were 3 GICs with > 30 A intensities. This second Halloween storm had the second-most GICs in the 21-year study. It should be noted that this second Halloween superstorm had a higher $SYM-H$ peak intensity than the first superstorm, but had fewer GICs in both intensity categories.

[Figure 4](#) shows a magnetic storm with peak intensity $SYM-H = -319$ nT associated with a complex corotating interaction region (CIR; [Smith & Wolfe, 1976](#); [Tsurutani et al., 1997, 2006](#)). The peak in the storm intensity occurred at ~0011 UT on day 98. An IMF B_s of intensity ~27 to ~32 nT was present from the shock (denoted by the vertical black dashed line) to the CIR interface at ~2316 UT day 97. This B_s caused the main phase of the storm. The strong shock at ~1643 UT (1943 LT) created only a sublevel GIC event. Mäntsälä was in the dusk-midnight sector at the time of shock impingement.

The shock also triggered a long-duration intense substorm with peak SML intensity of -2314 nT. A 20 A GIC occurred at the substorm peak.

A short-duration substorm of $SML = -1844$ nT at 2328 UT (day 97) is associated with a GIC intensity of 23 A.

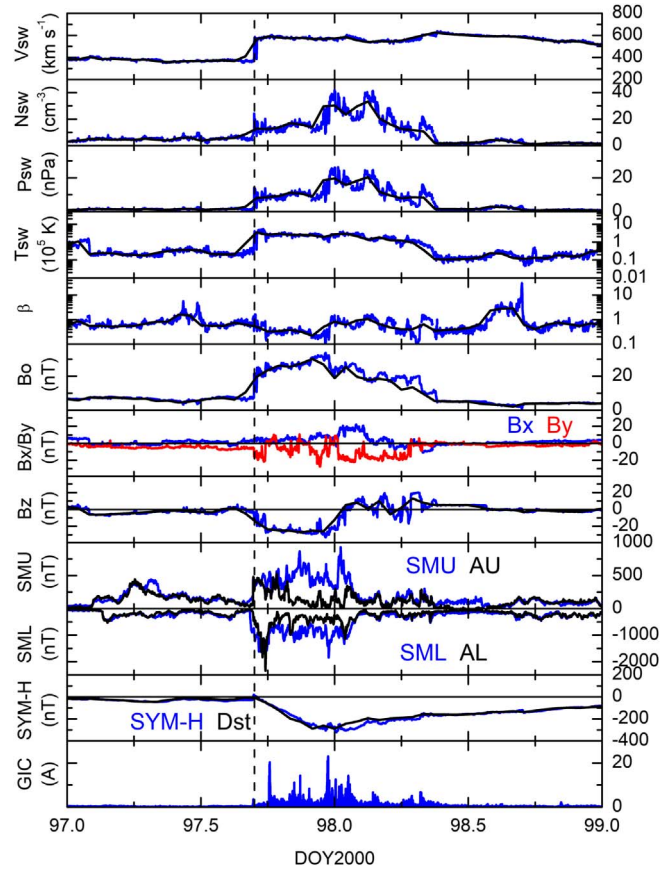


Fig. 4. The format is the same as for [Figure 2](#), but for days 97–98 (6–7 April), 2000.

The substorm spike is not present in the AL index, indicating that either the substorm was located at latitudes below Mäntsälä or that the substorm occurred at a longitude between the widely separated AL index stations. The substorm is coincident in time with an increase in solar wind ram pressure from ~ 9.5 to ~ 25.6 nPa. There were 16 GICs > 10 A intensities that occurred during these two days.

[Figure 5](#) shows an interplanetary sheath B_s causing a $SYM-H = -176$ nT magnetic storm. The storm peak occurred at ~ 2104 UT day 311. The shock is indicated by a vertical black dashed line at 0958 UT (1248 LT). The shock did not cause a GIC above the study threshold. Mäntsälä was in the noon sector at the time of shock arrival.

A 19 A GIC occurred at ~ 1807 UT on day 311 time-coincident with a solar wind PP with density $N_{SW} = 33 \text{ cm}^{-3}$ (shown by a vertical red dashed line). The upstream solar wind density prior to the PP was $\sim 5 \text{ cm}^{-3}$, so the ram pressure increase across the PP was a factor of ~ 6.6 times. This PP may be a coronal loop carried out to 1 AU. Such a high level of ram pressure increase is greater than most shock compressions. This GIC event is the largest for this interplanetary interval. Mäntsälä was in the dusk-midnight sector at the time of the GIC. There were only 3 GICs with > 10 A intensities on these two days.

In [Figure 6](#), the sheath B_s ahead of an ICME caused a magnetic storm of intensity $SYM-H = -101$ nT. The MC within the ICME had $B_z \sim 0$ nT, so it made the storm only slightly more

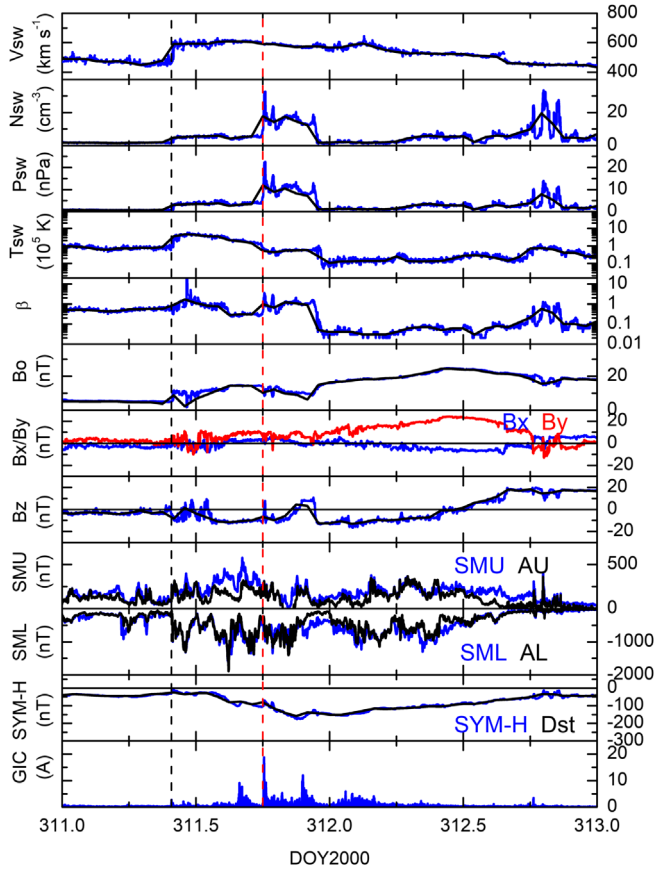


Fig. 5. The same format as in [Figure 2](#) except for days 311–312 (6–7 November, 2000). The vertical red dashed line indicates a PP occurrence.

intense. The storm peak occurred at ~0612 UT on day 22. There were 12 GICs with > 10 A intensities in these two days.

A strong shock at 1702 UT (2012 LT) on 21 January is denoted by a vertical black dashed line. The shock triggered a sharp onset of a SSS with peak *SML* value of -4418 nT. The shock or the SSS onset caused a GIC of 13 A. Mäntsälä was in the dusk-midnight sector at the time. During the decay phase of the SSS there was a large cluster of GICs reaching a peak intensity of 27 A at ~1910 UT. The peak GIC occurred at the same time as a sharp interplanetary density spike (PP) with a peak density of 55 cm $^{-3}$. The upstream density was ~ 11 cm $^{-3}$, thus the ram pressure increases was ~ 5 times. This is another example of an abrupt solar wind density increase causing an intense GIC.

There is another GIC of intensity 22 A at ~2015 UT on day 21. There is no obvious interplanetary phenomenon that appears to be the cause. There is no substorm feature at this time.

Following the 22 A GIC is a PP at ~2052 UT. This is associated with a heliospheric current sheet (HCS) crossing ([Smith et al., 1978](#)). The HCS is identified by sharp reversals in the sign of both IMF *Bx* and *By* components. This causes a GIC but below the 10 A threshold of this study.

[Figure 7](#) shows a different type of interplanetary event than the previous examples. This is a “slow” ICME where the peak solar wind speed *Vsw* is only ~ 520 km s $^{-1}$ (such slow ICMEs have been noted before: [Tsurutani et al., 2004](#)). There is no shock and sheath ahead of the ICME, but there is a “pileup”

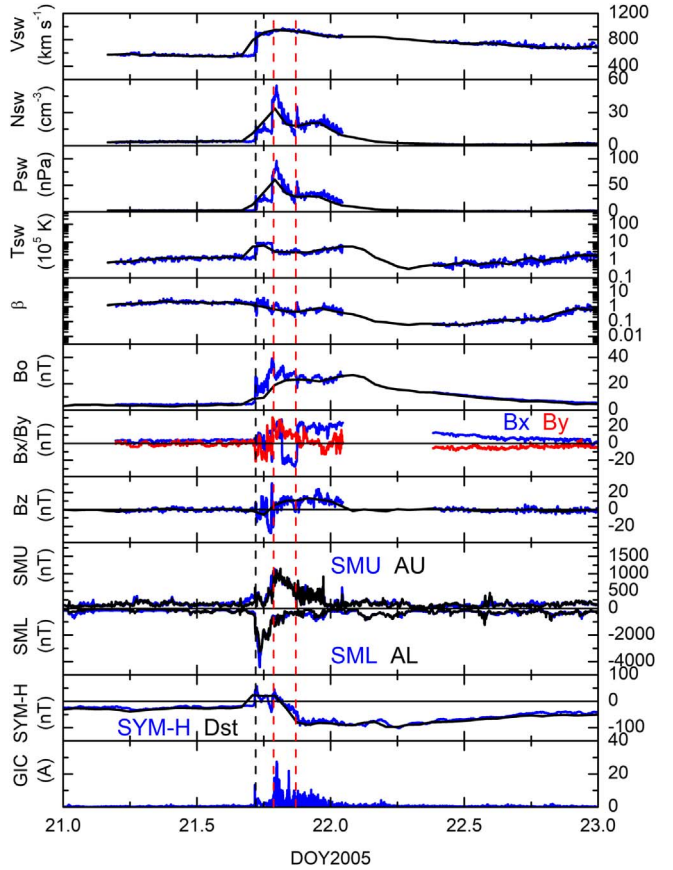


Fig. 6. The format is the same as in [Figure 2](#) but for days 21–22 (21–22 January, 2005). The vertical red dashed lines indicate PP events.

region there. The Bs in the pileup region causes a moderate magnetic storm of *SYM-H* peak = -61 nT. The MC *Bz* = 0 nT causes the lengthening of the storm main and recovery phases. During the storm main phase there are substorms with a peak *SML* value of -848 nT. There are no GICs above study threshold in this time interval.

An intense GIC of 20 A occurs at ~1924 UT on day 58. The cause of this is a sharp change of the IMF orientation from a *Bs* direction to a *Bn* direction (a *Bn* turning). This occurs at the boundary between the pileup region and the MC (*Bn* fields). There is also a solar wind ram pressure decrease at that time associated with the low plasma β of the MC. The IMF *Bn* turning terminates the substorm activity, so there is no substorm associated with this event.

[Figure 8](#) shows another different type of solar wind event, that of an interval of low solar wind speed *Vsw* with a peak value of only ~ 420 km s $^{-1}$. There is no shock/sheath, ICME (MC or filament), CIR or HSS involved in this event. Embedded within the low-speed solar wind is a long period *Bz* wave where the IMF *Bs* reaches ~ 23 nT. This southward IMF leads to a *SMY-H* = -153 nT magnetic storm. The storm peak occurs at ~1253 UT on day 274. There were 13 GICs with > 10 A intensities in these two days.

Throughout the relatively long main phase of the magnetic storm and in the beginning of the recovery phase, there is high and continuous substorm activity, noted by the *SML* indices. A double GIC event of 28 A and 19 A intensities occurs at

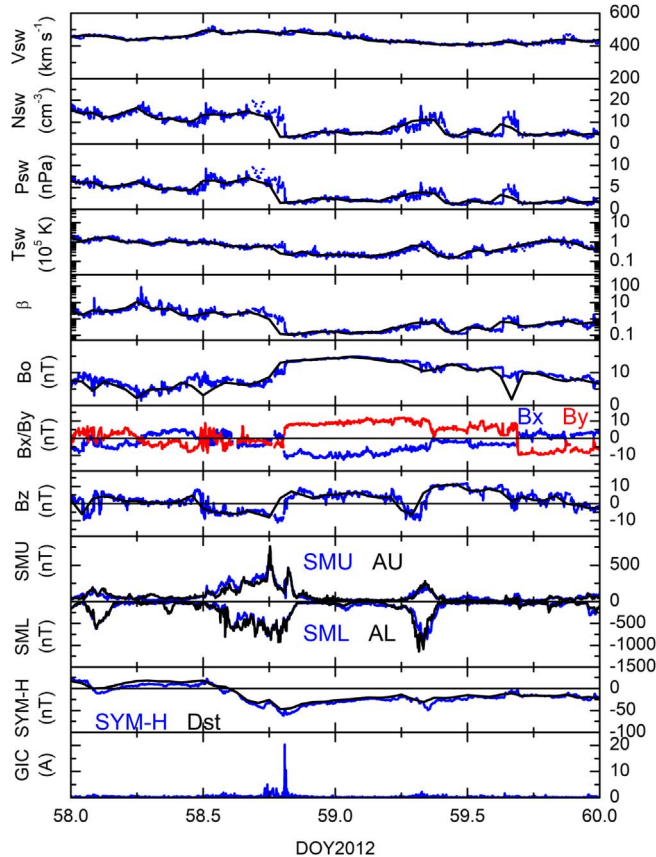


Fig. 7. The format is the same as in [Figure 2](#), but for days 58–59 (27–28 February, 2012).

~1629 UT and 1647 UT, respectively. This double GIC is associated with a short duration substorm spike of $SML = -1906$ nT. This occurred in the beginning of the storm recovery phase. There is no obvious interplanetary cause of this substorm. There is no particular IMF Bs or Bn turnings or Nsw features present at this time.

3.1 Analyses using all $GIC > 10$ A events

The [Appendix](#) shows all of the $GIC > 10$ A data in 48 plots ([Figs. A1 through A48](#)) and summaries. We use this full set of data to obtain some pertinent statistical information.

Almost all of the 48 event intervals were associated with geomagnetic storm intervals. About 21% were associated with superstorms ($SYM-H \leq -250$ nT), 60% with intense storms ($-250 \text{ nT} < SYM-H \leq -100$ nT), 17% with moderate storms ($-100 \text{ nT} < SYM-H \leq -50$ nT), and 2% with non-storms ($SYM-H > -50$ nT). Although the $GIC > 10$ A events were generally associated with storm intervals, they were not necessarily associated with magnetic storm main phases. Examples to the contrary were shown in [Figures 2 through 8](#). There are many such examples in the [Appendix](#).

GICs > 10 A were found to be associated with shocks, solar wind PPs, and IMF Bn and Bs turnings/intensifications. Many of the intense GIC events were associated with two or more interplanetary features.

To better understand the subset of interplanetary shock-related GICs > 10 A, the intensity and local times of all events

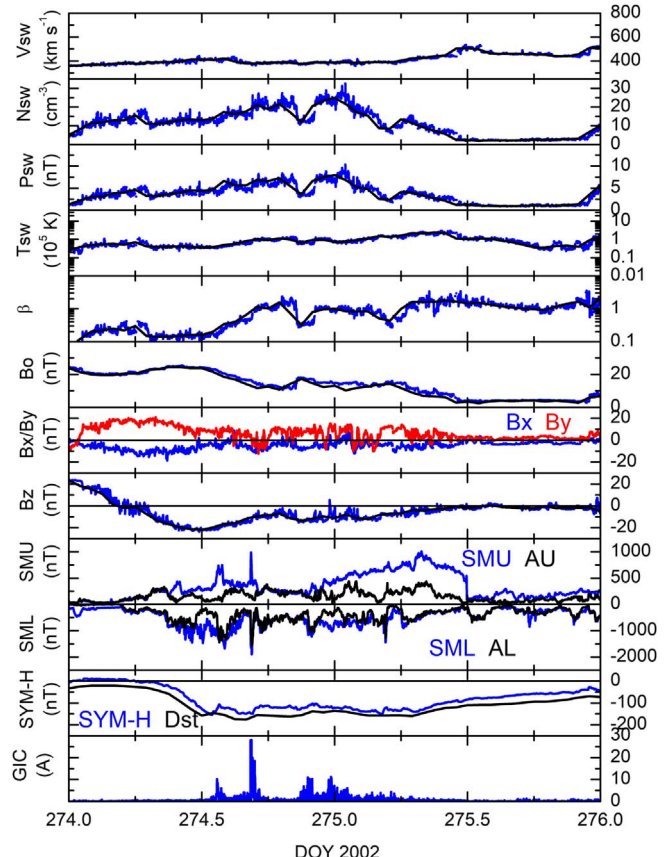


Fig. 8. The format is the same as in [Figure 2](#), but for days 274–275 (1–2 October, 2002).

are indicated in [Figure 9](#). Local noon is at the top of the figure and local midnight at the bottom. The GIC intensity scale is given on the left. It should be noted that all shocks caused a measurable GIC at Mäntsälä (see [Appendix](#) and [Figs. 2, 4, 5](#) and [6](#) for details), but typically below the 10 A level (there were over 300 shocks that occurred during the study interval). Events with below threshold intensities are not indicated in the above figure.

[Figure 9](#) shows that there were only 11 shock events (out of over ~ 300) that were time co-incident with GIC events above the 10 A level at Mäntsälä. Thus, in general, shocks are not geoeffective at high levels of GIC intensities. This is currently being studied to better understand this feature.

It is noted from [Figure 9](#) that shock-related GICs with intensities > 10 A can be detected at all local times. If only the most intense events are considered, there is a preference for morning and afternoon hours. However, it is noted that the largest event occurred near the dawn sector.

3.2 Analyses using all $GIC > 30$ A events

It is useful to identify the interplanetary and solar wind causes of the most intense GIC events, those with intensities of > 30 A. This value of > 30 A is an arbitrarily chosen one.

[Figure 10](#) and [Table 1](#) give the detailed information of all Mäntsälä GICs with > 30 A intensities. There are only $21 > 30$ A GIC events in the 21-year study period. Thus, these

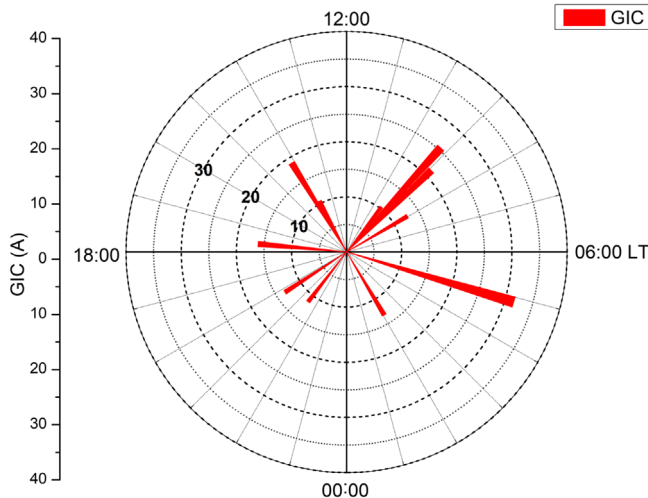


Fig. 9. Interplanetary shock-related Mäntsälä GIC >10 A events. The GIC intensity is indicated by the length of the red radius and the local time by the azimuth angle.

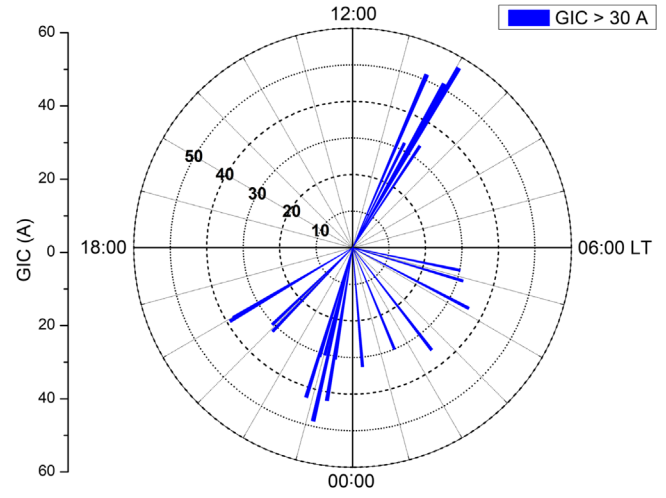


Fig. 10. Local time distribution and intensity of the > 30 A GIC events at Mäntsälä. The format is the same as in [Figure 9](#).

events are quite rare. One of these > 30 A events was related to a shock and six were related to ram pressure increases caused by PPs. [Figure 10](#) gives the information in a graphic format and [Table 1](#) in a tabular form. The plot format in [Figure 9](#) is the same as for [Figure 9](#) but here all > 30 A GICs are shown independent of whether they were shock-related or not.

The local time distribution of the GICs in [Figure 10](#) can be viewed as having two parts. There is a broad nightside distribution centered roughly at local midnight but extending from ~ 2000 LT to ~ 0500 LT. One might have the suspicion that these events may be substorm-related GICs. There is also a narrow region located in the morning-noon sector, ~ 1000 LT. These GIC events might be suspected to be PP-related events.

It should be noted that 4 of the events (with peaks 33 A, 57 A, 51 A, 52 A) at ~ 1000 LT GIC events are those from 29 to 30 October 2003, the first Halloween storm ([Table 1](#)). These events were associated with a SSS (see Discussion of [Fig. 2](#)). How does a substorm cause dayside GIC events?

Another one of the GIC events (32 A) at ~ 1000 LT is associated with a large solar wind PP on day 328, 2001 (see [Table 1](#) and [Fig. 3](#) discussion). So, we are seeing GICs (> 30 A) on the dayside associated with both substorms and PPs. It is clear that solar wind shocks and PPs could cause both dayside and nightside GICs. However, substorms causing dayside GICs are interesting and new and needs to be investigated further.

[Table 1](#) shows the details of the 21 > 30 A GIC events. The columns are, starting on the far left: the event interval (day-/year), the LT, the GIC intensity, the peak magnetic storm $SYM-H$ intensity, the related substorm peak SML intensity, and the peak solar wind density N_{sw} . The density value is only listed if an interplanetary PP was involved in the GIC event, thus the many blank boxes. The sixth column from the left indicates if an interplanetary PP or shock was related to an immediate GIC (a “Yes” response). If the PP or shock triggered a substorm and the substorm intensified with time and was later responsible for the GIC, a “No” is indicated. The next two columns indicate if the GIC is associated with an interplanetary sheath event or an ICME MC event.

There are several pertinent features that can be noted from the table. All of the events occurred between years from 2000 to 2004 and from 2012 to 2017. This corresponds to the solar cycle maximum to the declining phase for the first interval, and from the rising phase to the declining phase for the second interval (see the top panel of [Fig. 1](#) for reference to solar cycle phases). About half of the GIC > 30 A events are related to sheaths upstream of ICMEs and half to MCs within ICMEs. There were no CIRs involved with these 21 intense GIC events.

Of the 21 GIC > 30 A events, 16 (~76%) were related to superstorms ($SYM-H \leq -250$ nT). Sixteen (76%) of the GICs > 30 A were associated with either SSSs ($SML < -2500$ nT) or with intense (-2500 nT $< SML < -2000$ nT) substorms. There is one event associated with a shock/superstorm event (5%). The other 5 were associated with lesser intensity substorms. From all of the above, it is clear that GICs > 30 A events are associated with extremely intense magnetospheric and ionospheric geomagnetic activity.

4 Discussion and conclusions

4.1 Superstorms

Sixteen of the 21 Mäntsälä GIC > 30 A events were associated with superstorms ($SYM-H \leq -250$ nT). This does not mean that superstorms are causing the GICs, but that the enormous solar wind energy being pumped into the magnetosphere is leading to conditions conducive for the occurrence of particularly strong substorms. The prime examples for this were the first two Halloween storms on 29–30 and 30–31 October 2003 (see also [Viljanen et al., 2010](#) using a different data interval). Between the two superstorms, 9 GICs with intensities > 30 A and 258 GICs with intensities > 10 A occurred. These are good fractions (~43% and ~43%, respectively) of all of the events detected in the 21 years of study. It should be mentioned that these were not the largest magnetic storms. There were more intense storms with far fewer and considerably lower intensity GIC events. It is noted that the EUV solar flare (28 October 2003) related to the 29–30 October 2003

Table 1. Details of the GIC > 30 A events under study.

Day/year	LT	GIC peak (A)	SYM-H peak (nT)	SML peak (nT)	Nsw (cm ⁻³)	Shock/PP	Sheath	MC
197/2000	2302	30	-347	-3077	20.6	PP	No	Yes
310/2001	0453	32	-320	-2301		Shock	Yes	No
328/2001	1014	32	-233	-3839	65.0	No	No	No
302/2003	0946	33	-390	-3548		No	Yes	No
302/2003	0957	57	-390	-3548		No	Yes	No
302/2003	1003	51	-390	-3548		No	Yes	No
302/2003	1027	51	-390	-3548		No	Yes	No
303/2003	0130	30	-390	-2729		No	No	Yes
303/2003	0410	36	-390	-2340		No	No	Yes
303/2003	2309	49	-432	-3872	3.0	PP	Yes	No
304/2003	0019	33	-432	-2724	3.0	PP	Yes	No
304/2003	0513	30	-432	-807	3.0	PP	No	Yes
312/2004	0231	35	-392	-2071		No	No	Yes
314/2004	2251	43	-282	-2324		No	No	Yes
314/2004	2253	31	-282	-2324		No	No	Yes
314/2004	2322	42	-282	-2324		No	No	Yes
314/2004	2325	31	-282	-2324		No	No	Yes
075/2012	2001	38	-79	-1753	12.0	PP	Yes	No
075/2012	2003	39	-79	-1753	12.0	PP	Yes	No
076/2013	2105	32	-131	-990		No	Yes	No
251/2017	2055	30	-115	-1223		No	No	Yes

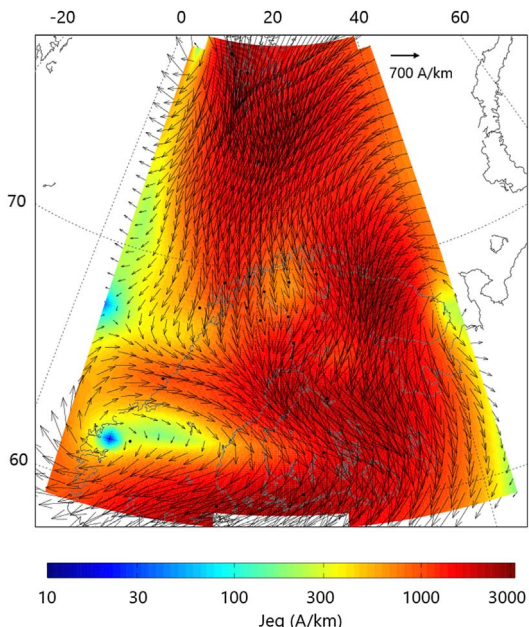


Fig. 11. Ionospheric equivalent currents between 59°N and 79°N latitudes and 3°E to 42°E longitudes obtained from the International Monitor for Auroral Geomagnetic Effects (IMAGE) of Space and Earth Observation Centre, Finnish Meteorological Institute (<https://space.fmi.fi/>) at 0657 UT on 29 October 2003 (the time of GIC peak of ~57 A). The color scale at the bottom shows the magnitude of the eastward currents. The ionospheric equivalent currents, flowing at ~100 km altitude, are calculated from 41 ground magnetometers (shown by black filled circles) from IMAGE.

Halloween storm was the most intense on record. This caused the greatest dayside flare-related ionospheric Total Electron Content (TEC) increase (~30%) on record (Tsurutani et al.,

2005). Mannucci et al. (2005) indicated that the 30–31 October 2003 Halloween superstorm had the largest dayside ionospheric “superfountain” uplift on record. Whether these ionospheric effects caused these two storms to have far more intense GIC events or not is unclear at this time.

Pulkkinen et al. (2005) reported high-voltage power transmission system failures in southern Sweden during the 30–31 October 2003 Halloween superstorm. The interplanetary cause of one GIC reported by Pulkkinen et al. (2005) was identified in this paper. It was a modest solar wind pressure pulse (PP) that created a large SI⁺ in SYM-H (+61 nT), a SML = -3872 nT SSS onset and a 49 A GIC at Mäntsälä, Finland (at 2249 LT). This GIC event was reported earlier relative to Figure 3 and is shown in Figure 10. This was the largest GIC event that occurred during the 30–31 October 2003 superstorm.

4.2 Substorms, intense substorms and SSSs

When one narrows the GICs to the most intense > 30 A events (Table 1), it is apparent that substorms play a major role. It can be noted that 16 of the 21 GIC > 30 A events are associated with intense substorms with SML < -2000 nT intensities. Nine of the events were SSSs (SML < -2500 nT). Substorms with such large intensities are relatively rare. The largest GIC was 57 A and was associated with a SSS (Fig. 10).

An event not covered in this study interval was the 1989 Hydro Quebec GIC-induced power outage. The magnetic storm was of superstorm intensity ($Dst = -589$ nT), even larger than any of the storm events covered in this study. Boteler (2019) recently concluded that a shock-triggered SSS caused the GIC which led to the collapse of the electric power grid. Earlier it was noted that magnetic storms were caused by intense magnetic reconnection between interplanetary Bs and the Earth's magnetopause magnetic fields. In this study we have found that shock triggering of intense substorms may initiate storms as well. Nightside injection of energetic plasma deep into the

magnetosphere will contribute to ring current enhancement and the storm. Possible examples are found in Figures 2, 4, A3, A4, A7 and A26.

4.3 Interplanetary PPs

From Table 1, it is noted that 6 out of the 21 Mäntsälä >30 A GICs were due to PPs. PPs being time-coincident with Mäntsälä GICs is a new discovery. PPs are the second most geoeffective interplanetary cause (after substorms) for >30 A GICs. Why were these PPs more geoeffective than shocks? The plasma density increase across a shock is a maximum of ~ 4 (Kennel et al., 1985), but statistically only a factor of 1–3 (Tsurutani & Lin, 1985). Several of the geoeffective PPs were noted to have considerably higher density increases than ~ 4 .

What are these interplanetary PP structures? It is possible that they are the high-density loops seen in coronagraph images when CMEs are close to the Sun. At 1 AU the coronal loops should appear between the upstream shock and the MC portion of the ICMEs. Events of this type are noted in Figures 5, A9, A18 and A32. Ion charge state analyses will be useful to verify this.

Could some of the PPs be ICME filaments? From the Lepri & Zurbuchen (2010) filament event interval list, only 2 of the 9 filament events coincided with our intervals of GICs with intensities > 10 A: on day 198, 2000 (Fig. A6) and on day 295, 2001 (Fig. A16). These filaments are shaded in the corresponding figures. Neither of the two filaments were associated with specific GICs above the study threshold.

We have identified other “possible” filaments which were geoeffective in producing Mäntsälä >10 A GICs. Because the events are of short durations, they could have easily been missed in the Lepri & Zurbuchen (2010) study. These PP events occurred on the sunward side of the MCs. In the text, we have used the modifier “possible” because we have not examined ion charge states data yet. And to further complicate matters, experts indicate that some filaments may not contain definitive ionic features. So, it is possible that we will not be able to obtain a final answer, even with further study.

Since PP impingements onto the magnetosphere is the same physical mechanism (an enhanced ram pressure pulse) as interplanetary shocks (the downstream enhanced densities sunward of forward shocks), it can be expected that PPs will cause GICs in the same locations as shocks have been noted to do: auroral latitudes, midlatitudes and at the equator. Future researchers should be aware of this new development.

4.4 Shocks

Shocks played a large role in the intense GIC events at Mäntsälä. There were 11 shock-related GICs > 10 A. However only one of these had an intensity > 30 A and thus shocks are apparently the third most important phenomena (after substorms and PP events) in this highest GIC intensity category.

There were over ~ 300 shocks identified in the study interval. It can be therefore concluded that shocks in general are not typically geoeffective at the Mäntsälä > 10 A level or > 30 A level. Of course, this is not to say that shock-induced GIC intensities could not be greater than found in this survey. Tsurutani & Lakhina (2014) have shown that considerable stronger shocks at the Earth are theoretically possible.

5 Final comments

In the literature, it has been assumed that dayside GICs associated with shock impingements onto the magnetosphere are due to a compressional wave propagating through the magnetosphere to the ionosphere causing dB/dt current events there (Araki et al., 1993; Tsurutani & Lakhina, 2014). However, there are other paths that the signals may take. It is known that shocks cause betatron acceleration of pre-existing dayside outer zone magnetospheric ~ 10 to 100 keV electrons and protons, accelerate the particles primarily in their perpendicular energies, leading to plasma instabilities (Kennel & Petschek, 1966; Tsurutani & Lakhina, 1997), plasma wave generation, and dayside auroral and subauroral and conductivity enhancements (Zhou & Tsurutani, 1999; Tsurutani et al., 2001a). If dayside auroral oval electric fields exist (Maezawa, 1976), a sudden ionospheric conductivity enhancement will cause dayside GICs much in the same way that the auroral electrojet on the nightside causes GICs. Interplanetary shock impingements also trigger nightside substorms (Heppner, 1955; Zhou & Tsurutani, 2001; Tsurutani & Zhou, 2003; Hajra & Tsurutani, 2018). So, at the present time if a shock impinges upon the magnetosphere and a GIC occurs at the same time, we are not certain which particular physical mechanism caused the GIC.

What is it about the auroral electrojet or auroral particle precipitation that causes the dB/dt at the surface of the Earth? Is it a rapid spatial motion of the electrojet current overhead? Or is it a sudden increase or decrease of that current (note that sudden current decreases also cause a dB/dt)? Or could it be due to sudden magnetic field-aligned precipitation of electrons or protons into the auroral ionosphere? Substorms involve rapid plasmashell injections, more spatially limited than that during magnetic storms (Tsurutani & Gonzalez, 2007). This injection can cause Pc5 and Ps6 pulsations. Which of these possibilities are the causes of GICs? At this time, we do not have answers. Possibly all of the above! And perhaps the causes are different for different substorm GIC events. To obtain definitive answers would require both detailed local magnetic field measurements and auroral all sky images to identify the dB/dt causes. This is beyond the scope of the present paper, but has been mentioned for readers interested in doing such detailed studies in the future.

In a converse sense we do not know how the nightside auroral ionospheric currents are connected to the dayside ionosphere. It has been shown that during HILDCAA (high-intensity long-duration continuous auroral activity, Tsurutani & Gonzalez, 1987) not only are the nightside and dayside auroral zones connected but there are auroras over the polar caps as well (Guarnieri, 2006; Guarnieri et al., 2006a, b). Plasma waves in the polar cap boundary layer show a continuous, unbroken oval circulating the magnetic pole (Tsurutani et al., 1998b, 2001b). Thus, does it make sense that a SSS originating on the nightside might expand and cause a GIC at ~ 1000 LT on the dayside? Or is it possible that the auroras and the electrojet were only present at ~ 1000 LT for the 29–30 October 2003 SSS? Zhou & Tsurutani (2004) noted dawn and dusk auroras during a high-speed solar wind stream. They suggested a mechanism of the Kelvin-Helmholz instability instead of magnetic reconnection for the solar wind energy input into the magnetosphere.

Figure 11 shows the equivalent ionospheric currents flowing at ~ 100 km altitude in the northern hemisphere at 0657 UT on

29 October 2003, corresponding to the ~ 57 A GIC at Mäntsälä (0957 LT). Strong currents of ~ 3000 A km^{-1} can be noted around Mäntsälä (60.6°N , 25.2°E geographic) during the GIC peak occurrence.

What is particularly striking about the ~ 57 A GIC event (and other > 30 A GICs during the first SSS of the 29 October 2003 superstorm) was that the GIC occurred when Mäntsälä was on the dayside (see discussion with Fig. 10)! This is not our traditional view of the Akasofu (1964) picture of substorms being confined to the midnight sector.

We mention that for a related event, a shock-triggered SSS ($SML = -4418$ nT) occurring on 21 January 2005, Hajra & Tsurutani (2018) showed that there was a general lack of auroral forms in the midnight sector, and intense auroras at dusk and at dawn. Unfortunately, the images did not go beyond dawn (in Fig. 2 of that paper). Figure 11 above clearly shows strong ionospheric currents flowing on the dayside during the 29 October 2003 SSS at 0657 UT that are most probably related to the intense GIC. It is possible that this may be a new type of “substorm”.

As previously mentioned, this paper is intended to be only a top-level survey. Much more detailed work is needed to understand the details of the physical causes of GICs. We hope, the reader will be encouraged to carry out such studies.

For pipeline mitigation techniques at auroral latitudes, we quote Campbell (1980) concerning the Alaska pipeline:

“Pipe corrosion occurs at the underground, exposed pipe points of coating holes and scratches where current can enter or leave the pipe. Such corrosion is proportional to the current density through the exposed points and decreases with the period of the current variation. The Alaska oil pipeline has been protected with sacrificial zinc electrodes that ground the pipe at regularly spaced intervals along the underground route to bleed the current away from the holes in the pipe coating.”

The Finnish natural gas pipeline mitigation technique is the same, using sacrificial electrodes (Pirjola & Lehtinen, 1985). For the Maritimes and Northeast pipeline in New England, they have used a slightly different technique because of the high resistivity of the soil in that region (Rix & Boteler, 2001). They have used “impressed current type cathode protection rather than passive anodes”. From reading some of the current literature (see Gummow & Eng, 2002; Popov & Lee, 2018; Googan, 2020), it seems that both of these techniques work quite well.

Concerning more equatorward latitude pipelines, during magnetic storms the electrojet comes down to midlatitudes. Fortunately, these events do not occur very often and when they do, they only last from a few hours to a few days (Gonzalez et al., 1994). Pipelines at subauroral latitudes are not nearly as vulnerable to magnetic storms as are electrical power systems.

Some pertinent comments from previous publications should be given to the readership concerning superstorms. It has been argued in Tsurutani et al. (2020) that it would take a very fast CME to cause a magnetic storm of the intensity of the Carrington 1–2 September 1859 storm (Tsurutani et al., 2003). The Carrington storm had an estimated intensity of $Dst \sim -1760$ nT, the largest in recorded history and ~ 3 times larger than the 1989 Hydro Quebec power outage. The transit time for the CME to go from

the Sun to Earth was ~ 17 h 40 min (Carrington, 1859). Thus Tsurutani et al. (2020) indicated that CME transit times less than 24 h would be most important for events of this type. We have identified the transit time of the 29–30 October 2003 CME. The elapsed time from observing the halo CME near Sun at ~ 1130 UT on 28 September (https://cdaw.gsfc.nasa.gov/CME_list/UNIVERSAL/2003_10/univ2003_10.html) to the detection of the fast forward shock at the Earth’s bow shock nose at ~ 0612 UT on 29 September, is ~ 19 h. Thus, it seems that CMEs with transit times of $< \sim 24$ h will be particularly geoeffective in causing GICs at subauroral latitudes. However as shown in the statistical results of this paper GICs at Mäntsälä and storm intensities do not have a one-to-one relationship. The general relationship is, however, good enough to use for forwarnings of possible GIC events. At this time we do not have enough knowledge to make more concrete predictions.

As mentioned previously, this paper is intended as a “top-level” survey. No effort was made to understand the “details” of the physical causes of GICs. To state that a “shock”, a “magnetic storm”, “a supersubstorm (SSS)” or “a plasma parcel (PP)” caused or was related to a GIC, is not a detailed understanding of the dB/dt that caused a particular GIC. More work needs to be done. But this indeed can be exciting for the young, energetic researchers who wish to make progress in this important field.

Acknowledgements. Portions of this effort were performed at the Jet Propulsion Laboratory, California Institute of Technology under contract with NASA. The work of R.H. is funded by the Science and Engineering Research Board (SERB), a statutory body of the Department of Science and Technology (DST), Government of India through the Ramanujan Fellowship. B.T.T. thanks Prof. A. Nishida for helpful scientific discussions. B.T.T. also thanks Prof. S.I. Akasofu for helpful scientific discussions. The Mäntsälä GIC data were collected from the Space and Earth Observation Centre of the Finnish Meteorological Institute (<https://space.fmi.fi/gic/index.php>). The solar wind and interplanetary magnetic field data were obtained from the OMNI website (<https://omniweb.gsfc.nasa.gov/>). The solar wind data for the 29–30 October and 30–31 October 2003 “Halloween storms” were obtained from R. Skoug. The geomagnetic $SYM-H$, Dst , AL and AU indices were obtained from the World Data Center for Geomagnetism, Kyoto, Japan (<http://wdc.kugi.kyoto-u.ac.jp/>). The SML and SMU indices were taken from the SuperMAG network (<http://supermag.jhuapl.edu/>). Ionospheric equivalent currents were obtained from the International Monitor for Auroral Geomagnetic Effects (IMAGE) of Space and Earth Observation Centre, Finnish Meteorological Institute (<https://space.fmi.fi/>). The editor thanks two anonymous reviewers for their assistance in evaluating this paper.

References

- Akasofu SI. 1964. The development of the auroral substorm. *Planet Space Sci* **12**: 273–282. [https://doi.org/10.1016/0032-0633\(64\)90151-5](https://doi.org/10.1016/0032-0633(64)90151-5).
- Araki T, Funato K, Iguchi T, Kamei T. 1993. Direct detection of solar wind dynamic pressure effect on ground geomagnetic field. *Geophys Res Lett* **20**: 775–778. <https://doi.org/10.1029/93GL00852>.

- Barlow WH. 1849. On the spontaneous electrical currents observed in the wires of the electric telegraph. *Phil Trans R Soc Lond* **139**: 61–72. <https://doi.org/10.1098/rstl.1849.0006>.
- Boteler DH. 2019. A 21st century view of the March 1989 magnetic storm. *Space Weath* **17**: 1427–1441. <https://doi.org/10.1029/2019SW02278>.
- Burlaga L, Sittler E, Mariani F, Schwenn R. 1981. Magnetic loop behind an interplanetary shock: Voyager, Helios, and IMP 8 observations. *J Geophys Res* **86**: 6673–6684. <https://doi.org/10.1029/JA086iA08p06673>.
- Burlaga L, Fitzenreiter R, Lepping R, Ogilvie K, Szabo A, Lazarus A, Steinberg J, Gloeckler G, Howard R, Michels D, Farrugia C, Lin RP, Larson DE. 1998. A magnetic cloud containing prominence material: January 1997. *J Geophys Res* **103**: 277–285. <https://doi.org/10.1029/97JA02768>.
- Campbell WH. 1980. Observation of electric currents in the Alaska oil pipeline resulting from auroral electrojet current sources. *Geophys J R Astr Soc* **61**: 437–449. <https://doi.org/10.1111/j.1365-246X.1980.tb04325.x>.
- Carrington RC. 1859. Description of a singular appearance seen in the Sun on September 1, 1859. *Mon Not R Astron Soc*, **XX**: 13–15.
- Chen PF. 2011. Coronal mass ejections: Models and their observational basis. *Living Rev Solar Phys* **8**: 1–92. <http://www.livingreviews.org/lrsp-2011-1>.
- Daglis IA, Thorne RM, Baumjohann W, Orsini S. 1999. The terrestrial ring current: formation and decay. *Rev Geophys* **37**: 407–438.
- Du AM, Tsurutani BT, Sun W. 2008. Anomalous geomagnetic storm of 21–22 January 2005: A storm main phase during northward IMFs. *J Geophys Res* **113**: A10214. <https://doi.org/10.1029/2008JA013284>.
- Dungey JW. 1961. Interplanetary magnetic field and the auroral zones. *Phys Rev Lett* **6**: 47–50.
- Echer E, Gonzalez WD, Tsurutani BT. 2008a. Interplanetary conditions leading to superintense geomagnetic storms ($Dst \leq -250$ nT) during solar cycle 23. *Geophys Res Lett* **35**: L06S03. <https://doi.org/10.1029/2007GL031755>.
- Echer E, Gonzalez WD, Tsurutani BT, Gonzalez ALC. 2008b. Interplanetary conditions causing intense geomagnetic storms ($Dst \leq -100$ nT) during solar cycle 23 (1996–2006). *J Geophys Res* **113**: A05221. <https://doi.org/10.1029/2007JA012744>.
- Farrugia CJ, Erkaev NV, Biernat HK, Burlaga LF, Lepping RP, Osherovich VA. 1997. Possible plasma depletion layer ahead of an interplanetary ejecta. *J Geophys Res* **102**: 7087–7093. <https://doi.org/10.1029/96JA03822>.
- Gonzalez WD, Tsurutani BT. 1987. Criteria of interplanetary parameters causing intense magnetic storms ($Dst < -100$ nT). *Planet Space Sci* **35**: 1101–1109. [https://doi.org/10.1016/0032-0633\(87\)90015-8](https://doi.org/10.1016/0032-0633(87)90015-8).
- Gonzalez WD, Tsurutani BT, Gonzalez ALC, Smith EJ, Tang F, Akasofu SI. 1989. Solar wind-magnetosphere coupling during intense magnetic storms (1978–1979). *J Geophys Res* **94**: 8835–8851. <https://doi.org/10.1029/JA094iA07p08835>.
- Gonzalez WD, Joselyn JA, Kamide Y, Kroehl HW, Rostoker G, Tsurutani BT, Vasylunas VM. 1994. What is a geomagnetic storm? *J Geophys Res* **99**: 5771–5792. <https://doi.org/10.1029/93JA02867>.
- Gonzalez WD, Echer E, Gonzalez ALC, Tsurutani BT. 2007. Interplanetary origin of intense geomagnetic storms ($Dst \leq -100$ nT) during solar cycle 23. *Geophys Res Lett* **34**: L06101. <https://doi.org/10.1029/2006GL028879>.
- Googan C. 2020. The cathodic protection potential criteria: Evaluation of the evidence. *Mat Corr*. <https://doi.org/10.1002/maco.202011978>.
- Guarnieri FL. 2006. The nature of auroras during High-Intensity Long-Duration Continuous AE Activity (HILDCAA) events: 1998 to 2001. In: *Recurrent Magnetic Storms: Corotating Solar Wind Streams*, vol. **167**, Tsurutani BT, et al., (Eds.) Geophys. Mon. Ser., Amer. Geophys., Un. Press, Washington DC. pp. 235–243. <https://doi.org/10.1029/167GM19>
- Guarnieri FL, Tsurutani BT, Echer E, Gonzalez WD. 2006a. Geomagnetic activity and auroras caused by high-speed streams: A review. In: *Adv Geosci*, Vol. **8**, edited by Duldig et al., World Sci Publ. Co. pp. 91–102.
- Guarnieri FL, Tsurutani BT, Gonzalez WD, Gonzalez ALC, Grande M, Soraas F, Echer E. 2006b. ICME and CIR storms with particular emphases on HILDCAA events. In: *ILWS Workshop 2006, GOA*.
- Gummow RA, Eng P. 2002. GIC effects on pipeline corrosion and corrosion control systems. *J Atmos Sol-Terr Phys* **64**: 1755–1764.
- Hajra R, Tsurutani BT. 2018. Interplanetary shocks inducing magnetospheric supersubstorms ($SML < -2500$ nT): Unusual auroral morphologies and energy flow. *Astrophys J* **858**: 123. <https://doi.org/10.3847/1538-4357/aabaed>.
- Heppner JP. 1955. Note on the occurrence of worldwide SSCs during the onset of negative bays at College, Alaska. *J Geophys Res* **60**: 29–32. <https://doi.org/10.1029/JZ060i001p00029>.
- Illing RME, Hundhausen AJ. 1986. Disruption of a coronal streamer by an eruptive prominence and coronal mass ejection. *J Geophys Res* **91**: 10951–10960. <https://doi.org/10.1029/JA091iA10p10951>.
- Kennel CF, Petschek HE. 1966. Limit on stable trapped particle fluxes. *J Geophys Res* **71**: 1–28. <https://doi.org/10.1029/JZ071i001p00001>.
- Kennel CF, Scarf FL, Coroniti FV, Russell CT, Wenzel K-P, Sanderson TR, Van Ness P, Feldman WC, Parks GK, Smith EJ, Tsurutani BT, Mozer FS, Temerin M, Anderson RR, Scudder JD, Scholer M. 1984a. Plasma and energetic particle structure upstream of a quasi-parallel interplanetary shock. *J Geophys Res* **89**: 5419–5435.
- Kennel CF, Edmiston JP, Scarf FL, Coroniti FV, Russell CT, Smith EJ, Tsurutani BT, Scudder JD, Feldman WC, Anderson RR, Mozer FS, Temerin M. 1984b. Structure of the November 12, 1978, quasi-parallel interplanetary shock. *J Geophys Res* **89**: 5436–5452. <https://doi.org/10.1029/JA089iA07p05436>.
- Kennel CF, Edmiston JP, Hada T. 1985. A quarter century of collisionless shock research. In: *Collisionless Shocks in the Heliosphere: a Tutorial Review*, vol. **34**, Stone RG, Tsurutani BT, (Eds.) Amer. Geophys., Un. Press, Washington DC. pp. 1. <https://doi.org/10.1029/GM034p0001>
- Lepri ST, Zurbuchen TH. 2010. Direct observational evidence of filamentary material within interplanetary coronal mass ejections. *Astrophys J Lett* **723**: L22–L27. <https://doi.org/10.1088/2041-8205/723/1/L22>.
- Maezawa K. 1976. Magnetospheric convection induced by the positive and negative z components of the interplanetary magnetic field: Quantitative analysis using polar cap magnetic records. *J Geophys Res* **81**: 2289–2303. <https://doi.org/10.1029/JA081i013p02289>.
- Mannucci AJ, Tsurutani BT, Iijima BA, Komjathy A, Saito A, Gonzalez WD, Guarnieri FL, Kozyra JU, Skoug R. 2005. Dayside global ionospheric response to the major interplanetary events of October 29–30, 2003 “Halloween storms”. *Geophys Res Lett* **32**: L12S02. <https://doi.org/10.1029/2004GL021467>.
- Meng C-I, Tsurutani B, Kawasaki K, Akasofu S-I. 1973. Cross-correlation analysis of the AE index and the interplanetary magnetic field Bs component. *J Geophys Res* **78**: 617–628.
- Meng X, Tsurutani BT, Mannucci AJ. 2019. The solar and interplanetary causes of superstorms (Minimum $Dst \leq -250$ nT) during the space age. *J Geophys Res* **124**: 3926–3948. <https://doi.org/10.1029/2018JA026425>.

- Pirjola R, Lehtinen M. 1985. Currents produced in the Finnish 400 kV power transmission grid and in the Finnish natural gas pipeline by geomagnetically-induced electric fields. *Ann Geophys* **3**: 485–491.
- Popov BN, Lee J-W. 2018. Cathodic protection of pipelines. In: *Handbook of Environmental Degradation of Materials*, Elsevier. <https://doi.org/10.1016/B978-0-323-52472-8.00025-3>.
- Pulkkinen A, Viljanen A, Pajunpaa K, Pirjola R. 2001. Recordings and occurrence of geomagnetically induced currents in the Finnish natural gas pipeline network. *J Appl Geophys* **48**: 219–231. [https://doi.org/10.1016/S0926-9851\(01\)00108-2](https://doi.org/10.1016/S0926-9851(01)00108-2).
- Pulkkinen A, Lindahl S, Viljanen A, Pirjola R. 2005. Geomagnetic storm of 29–31 October 2003: Geomagnetically induced currents and their relation to problems in the Swedish high-voltage power transmission system. *Space Weath* **3**: S08C03. <https://doi.org/10.1029/2004SW000123>.
- Rix BC, Boteler DH. 2001. Telluric current considerations in the design for the Maritimes and Northeast pipeline. In: *Paper presented at the Corrosion 2001*, Houston, Texas, March 2001.
- Smith EJ, Wolfe JH. 1976. Observations of interaction regions and corotating shocks between one and five AU: Pioneers 10 and 11. *Geophys Res Lett* **3**: 137–140.
- Smith EJ, Tsurutani BT, Rosenberg RL. 1978. Observations of the interplanetary sector structure up to heliographic latitudes of 16: Pioneer 11. *J Geophys Res* **83(A2)**: 717–724.
- Stone RG, Tsurutani BT. 1985. *Collisionless shocks in the heliosphere: A tutorial review*. Am Geophys Un Mon Ser (AGU), vol 35, Washington DC.
- Tsurutani BT, Gonzalez WD. 1987. The causes of high-intensity long-duration continuous AE activity (HILDCAAs): interplanetary Alfvén wave trains. *Planet Space Sci* **35**: 405–412. [https://doi.org/10.1016/0032-0633\(87\)90097-3](https://doi.org/10.1016/0032-0633(87)90097-3).
- Tsurutani BT, Gonzalez WD. 1995. The efficiency of viscous interaction between the solar wind and the magnetosphere during intense northward IMF events. *Geophys Res Lett* **22**: 663–666. <https://doi.org/10.1029/95GL00205>.
- Tsurutani BT, Gonzalez WD. 1997. The interplanetary causes of magnetic storms: A review. In: *Magnetic Storms*, vol. **98**, Tsurutani BT, Gonzalez WD, Amer. Geophys., Un. Press, Washington DC. pp. 77. <https://doi.org/10.1029/GM098p0077>.
- Tsurutani BT, Gonzalez WD. 2007. A new perspective on the relationship between substorms and magnetic storms. In: *Adv. Geosci.*, Vol. **8**, Sol. Terr., edited by M. Duldig et al., World Sci. Publ. Co., pp. 1–21.
- Tsurutani BT, Lakhina GS. 1997. Some basic concepts of wave-particle interactions in collisionless plasmas. *Rev Geophys* **35**: 491–502.
- Tsurutani BT, Lakhina GS. 2014. An extreme coronal mass ejection and consequences for the magnetosphere and Earth. *Geophys Res Lett* **41**: 287–292. <https://doi.org/10.1002/2013GL058825>.
- Tsurutani BT, Lin RP. 1985. Acceleration of > 47 keV ions and > 2 keV electrons by interplanetary shocks at 1 AU. *J Geophys Res* **90**: 1–11.
- Tsurutani BT, Meng C-I. 1972. Interplanetary magnetic-field variations and substorm activity. *J Geophys Res* **77**: 2964–2970.
- Tsurutani BT, Stone RG. 1985. Collisionless shocks in the heliosphere: Review of current research. In: *Amer Geophys*, Vol. **34**, Un. Press: Washington, DC.
- Tsurutani BT, Zhou XY. 2003. Interplanetary shock triggering of substorms: WIND and POLAR. *Adv Space Res* **31**: 1063–1067. [https://doi.org/10.1016/S0273-1177\(02\)00796-2](https://doi.org/10.1016/S0273-1177(02)00796-2).
- Tsurutani BT, Gonzalez WD, Tang F, Akasofu SI, Smith EJ. 1988. Origin of interplanetary southward magnetic fields responsible for major magnetic storms near solar maximum (1978–1979). *J Geophys Res* **95**: 8519–8531. <https://doi.org/10.1029/JA093iA08p08519>.
- Tsurutani BT, Gonzalez WD, Tang F, Lee YT. 1992. Great magnetic storms. *Geophys Res Lett* **19**: 73–76. <https://doi.org/10.1029/91GL02783>.
- Tsurutani BT, Kamide Y, Gonzalez WD, Arballo JK. 1997. Magnetic Storms. *Amer. Geophys.* Un. Press, Washington DC. pp. 98.
- Tsurutani BT, Arballo JK, Lakhina GS, Ho CM, Ajello J, Pickett JS, Gurnett DA, Lepping RP, Peterson WK, Rostoker G, Kamide Y, Kokubun S. 1998a. The January 10, 1997 auroral hot spot, horseshoe aurora and first substorm: A CME loop? *Geophys Res Lett* **25**: 3047–3050. <https://doi.org/10.1029/98GL01304>.
- Tsurutani BT, Lakhina GS, Ho CM, Arballo JK, Galvan C, Boonsiriseth A, Pickett JS, Gurnett DA, Peterson WK, Thorne RM. 1998b. Broadband plasma waves observed in the polar cap boundary layer: POLAR. *J Geophys Res* **103**: 17351–17366. <https://doi.org/10.1029/97JA03063>.
- Tsurutani BT, Zhou XY, Vasylunas VM, Haerendel G, Arballo JK, Lakhina GS. 2001a. Interplanetary shocks, magnetopause boundary layers and dayside auroras: The importance of a very small magnetospheric region. *Surv. Geophys.* **22**: 101–130, Kluwer Publ., Netherlands. <https://doi.org/10.1023/A:1012952414384>.
- Tsurutani BT, Arballo JK, Galvan C, Zhang LD, Zhou XY. 2001b. Polar cap boundary layer waves: An auroral zone phenomenon. *J Geophys Res* **106**: 19035–19055. <https://doi.org/10.1029/2000JA003007>.
- Tsurutani BT, Gonzalez WD, Lakhina GS, Alex S. 2003. The extreme magnetic storm of 1–2 September 1859. *J Geophys Res* **108**: 1268. <https://doi.org/10.1029/2002JA009504>.
- Tsurutani BT, Gonzalez WD, Guarneri F, Kamide Y, Zhou X, Arballo JK. 2004. Are high-intensity long-duration continuous AE activity (HILDCAA) events substorm expansion events? *J Atmos Sol Terr Phys* **66**: 167–176. <https://doi.org/10.1016/j.jastp.2003.08.015>.
- Tsurutani BT, Judge DL, Guarneri FL, Gangopadhyay P, Jones AR, Nuttal J, Zambon GA, Didkovsky L, Mannucci AJ, Iijima B, Meier RR, Immel TJ, Woods TN, Prasad S, Floyd L, Huba J, Solomon SC, Straus P, Viereck R. 2005. The October 28 2003 extreme EUV solar flare and resultant extreme ionospheric effects: Comparison to other Halloween events and the Bastille Day event. *Geophys Res Lett* **32**: L03S09. <https://doi.org/10.1029/2004GL021475>.
- Tsurutani BT, McPherron RL, Gonzalez WD, Lu G, Sobral JHA, Gopalswamy N. 2006. Corotating solar wind streams and recurrent geomagnetic activity. *Am. Geophys.*, Un. Press, Washington DC. pp. 167.
- Tsurutani BT, Lakhina GS, Verkhoglyadova OP, Gonzalez WD, Echer E, Guarneri FL. 2011. A review of interplanetary discontinuities and their geomagnetic effects. *J Atmos Sol Terr Phys* **73**: 5–19. <https://doi.org/10.1016/j.jastp.2010.04.001>.
- Tsurutani BT, Hajra R, Echer E, Gjerloev JW. 2015. Extremely intense ($SML \leq 22122500$ nT) substorms: isolated events that are externally triggered? *Ann Geophys* **22**: 519–524. <https://doi.org/10.5194/angeo-33-519-2015>.
- Tsurutani BT, Lakhina GS, Hajra R. 2020. The physics of space weather/solar-terrestrial physics (STP): what we know now and what the current and future challenges are. *Non Proc Geophys* **27**: 75–119. <https://doi.org/10.5194/npg-27-75-2020>.
- Viljanen A, Pulkkinen A, Pirjola R, Pajunpaa K, Posio P, Koistinen A. 2006. Recordings of geomagnetically induced currents and a nowcasting service of the Finnish natural gas pipeline system. *Space Weath* **4**: S10004. <https://doi.org/10.1029/2006SW000234>.
- Viljanen A, Koistinen A, Pajunpää K, Pirjola R, Posio P, Pulkkinen A. 2010. Recordings of geomagnetically induced currents in the finnish natural gas pipeline – Summary of an 11-year Period. *Geophysica* **46**: 59–67.

- Williams DJ. 1985. Dynamics of the Earth's ring current: theory and observation. *Space Sci Rev* **42**: 375–396. <https://doi.org/10.1007/BF00214994>.
- Zhang J, Richardson IG, Webb DF, Gopalswamy N, Huttunen E, Kasper JC, Nitta NV, Poomvises W, Thompson BJ, Wu CC, Yahir S, Zhukov AN. 2007. Solar and interplanetary sources of major geomagnetic storms ($Dst \leq -100$ nT) during 1996–2005. *J Geophys Res* **112**: A10102. <https://doi.org/10.1029/2007JA012321>.
- Zhou X, Tsurutani BT. 1999. Rapid intensification and propagation of the dayside aurora: Large scale interplanetary pressure pulses (fast shocks). *Geophys Res Lett* **26**: 1097–1100. <https://doi.org/10.1029/1999GL900173>.
- Zhou X, Tsurutani BT. 2001. Interplanetary shock triggering of nightside geomagnetic activity: Substorms, pseudobreakups, and quiescent events. *J Geophys Res* **116**: 18957–18967. <https://doi.org/10.1029/2000JA003028>.
- Zhou X, Tsurutani BT. 2004. Dawn and dusk auroras caused by gradual solar wind ram pressure events. *J Atmos Sol Terr Phys* **66**: 153–160.

Appendix

In the narrative below, we discuss the interplanetary and magnetospheric/ionospheric features time-coincident with the Mäntsälä, Finland geomagnetically induced current (GIC) events with intensities > 10 A. We show the interplanetary data so that the readership can note the relationship between GICs > 10 A and their interplanetary causes. The figures and related text will also describe the Mäntsälä GICs in relation to geomagnetic storm and substorm activity. Many of the GIC events occur before, during, or after magnetic storms, so a broad swath of relevant interplanetary data is shown for each event.

Day 13 (13 January), 1999 (Fig. A1). A CIR caused double dip storm with $SYM-H$ peak value of -111 nT. The two long-duration substorms caused the double dip storm. There is a small sublevel GIC with the forward shock which occurred at ~ 1054 UT (1354 LT). At the time Mäntsälä was in the afternoon sector. A sharp B_s increase caused the second dip of the storm and a $SML = -1189$ nT peak long-duration substorm. A GIC cluster with 10 A and 13 A peak intensity events occurred near the end of the substorm with a sharp SMU increase to 469 nT. The storm recovery phase begins after this last substorm.

Day 49 (18 February), 1999 (Fig. A2). Double dip magnetic storm of intensity $SYM-H = -128$ nT (in first dip). The storm is caused by the sheath B_s . The MC causes the second storm dip. A shock occurred at ~ 0247 UT (0547 LT) and caused a sublevel GIC. At the time Mäntsälä was in the dawn sector. There was a GIC cluster with peak 12 A event at the beginning of the storm second dip recovery phase. The GIC cluster was associated with a substorm with intensity $SML = -1604$ nT.

Days 265–266 (22–23 September), 1999 (Fig. A3). Two shocks, two sheaths, and a MC event. The second sheath B_s caused both a storm of intensity $SYM-H = -166$ nT and a long-duration substorm of $SML = -1608$ nT. The shocks at ~ 1223 UT (1523 LT) and ~ 1942 UT (2242 LT) created sublevel GIC events. At the times of the two shocks Mäntsälä was in the afternoon and midnight sectors, respectively. Although the

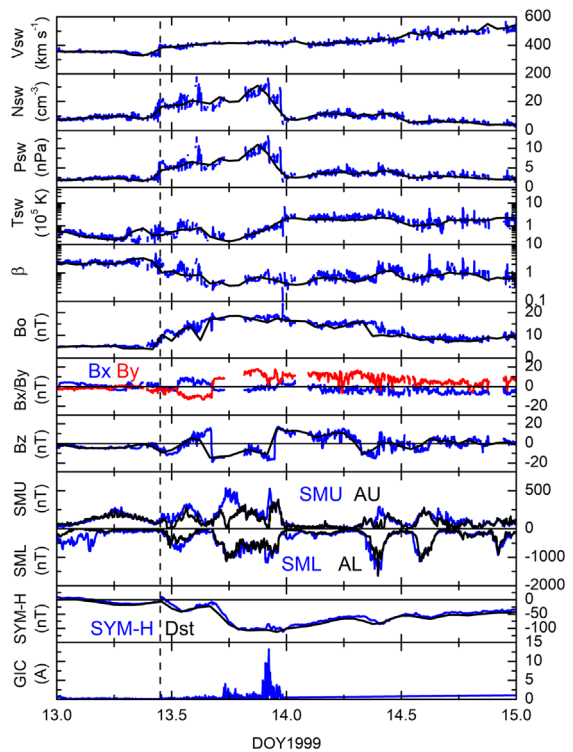


Fig. A1. Events on day 13 (13 January) 1999. From top down are the solar wind velocity (V_{sw}), density (N_{sw}), ram pressure (P_{sw}), temperature (T_{sw}), plasma β , magnetic field magnitude (B_o), the B_x and B_y components (in the same panel) and B_z in GSM coordinates. The bottom four panels are the SMU and AU (in the same panel), SML and AL (in the same panel), $SYM-H$ and Dst (in the same panel) and the GIC intensities. In the solar wind/interplanetary and geomagnetic indices panels, blue and black curves show 1 min and 1 h resolution data, respectively. The vertical black dashed line indicates the time of the interplanetary shock.

second sheath B_s appears to have caused the magnetic storm, the substorm may have contributed greatly. A cluster of GICs is related to the substorm but there is only one event above threshold, 11 A. The GIC cluster occurs during the storm main phase and the start of the recovery phase (at the end of the substorm).

Days 97–98 (6–7 April), 2000 (Fig. A4). This event was previously discussed in Results section (Fig. 4). A complex CIR associated superstorm with peak intensity $SYM-H = -319$ nT at ~ 0011 UT day 98. There was a \sim constant B_s of intensity ~ 30 nT from the shock to the CIR interface at ~ 2316 UT day 97. The shock triggered a long-duration intense substorm with peak SML intensity of -2314 nT. This intense substorm contributed to the storm initial intensification. The strong shock at ~ 1643 UT (1943 LT) created a sublevel GIC event. Mäntsälä was in dusk sector at the time. A 20 A GIC occurs at the substorm peak several hours later. A second peak GIC of 23 A was associated with a short duration substorm of $SML = -1844$ nT intensity at 2328 UT day 97 in the storm main phase. This substorm spike was not present in the AL indices. The substorm is coincident in time with a solar wind ram pressure increase to ~ 26 nPa. The high solar wind densities on the

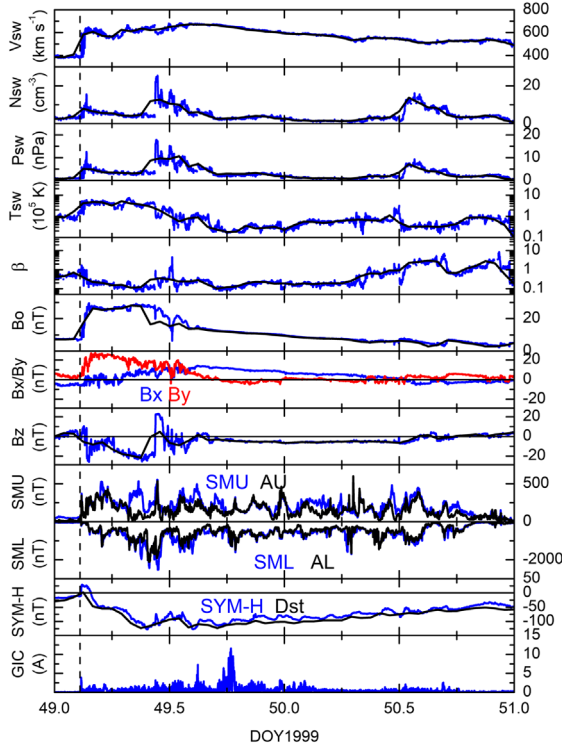


Fig. A2. Events on day 49 (18 February) 1999. Same format as in Figure A1.

solar side of the interface of the CIR is unusual. $16 > 10$ A GICs occurred during this interval.

Day 145 (May 24), 2000 (Fig. A5). A complex CIR causes a magnetic storm of peak intensity $SYM-H = -173$ nT. The main phase of the storm is caused by a long-duration intense substorm with $SML = -2121$ nT peak intensity. The substorm causes a GIC cluster with two events of 10 A and 11 A intensities.

Day 197–198 (July 15–16), 2000 (Fig. A6). A $SYM-H = -347$ nT superstorm caused by Bs fields in the upstream sheath and following MC Bs fields. A 16 A GIC is associated with the shock/short-duration $SML = -2112$ nT intense substorm (the shock is noted by a SI^+ of 84 nT at ~1439 UT (1739 LT) (the interplanetary data is low resolution for this part of the event). At the time of the shock, Mäntsälä was in the dusk sector. There are many more intense substorms after the shock but no corresponding GICs above the study threshold. The biggest GIC spike of 30 A occurs in beginning of the storm main phase and the decay phase of a short-duration SSS of SML intensity -3077 nT at 1901 UT (2201 LT). Mäntsälä was in the dusk-midnight sector at the time. In the storm recovery phase, there is a 17 A GIC associated with a $SML = -1033$ nT substorm. There were $30 > 10$ A GICs during this event. At ~1200 UT day 198, there is an ICME filament indicated by the vertical shading. It is associated with small GICs below the study threshold.

Days 261–262 (17–18 September), 2000 (Fig. A7). A sheath event (without shocks) Bs caused a $SYM-H = -203$ nT storm.

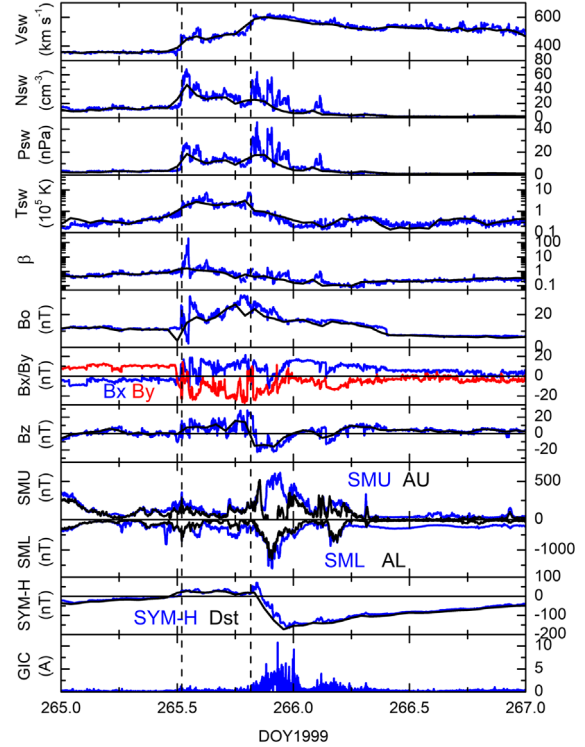


Fig. A3. Events on days 265–266 (22–23 September) 1999. Same format as in Figure A1.

A long-duration intense substorm of $SML = -2216$ nT (or the Bs) caused the storm main phase and also a GIC cluster with 2 peak intensities of 13 A and 14 A. A GIC of intensity 15 A occurred at the end of the intense substorm, coincident with an IMF Bs-to-Bn turning. GICs of 13 A at 0342 UT (0642 LT) and 13 A at 1001 UT (1301 LT) on day 262 were present in the storm recovery phase. Both were not associated with any obviously related substorm or interplanetary feature.

Days 278–279 (4–5 October), 2000 (Fig. A8). Two shocks and two sheaths caused a $SYM-H = -187$ nT triple dip storm. The weak shock at ~1413 UT (1713 LT) and pre-existing Bs fields formed the first -185 nT storm. The shock created a substorm of intensity $SML = -1435$ nT and a GIC of sublevel intensity. The second shock occurred at 0326 UT (0626 LT) on day 279 and caused a sublevel GIC. The second sheath Bs interval creates a $SYM-H = -187$ nT storm and a substorm of $SML = -1947$ nT. A second interval of sheath IMF Bs created a SSS of $SML = -2787$ nT and the third (but lesser) dip of the storm. The SSS does not cause a GIC with intensities above threshold. In the storm recovery phase, there is a short-duration substorm with SML peak intensity of only -1158 nT that causes a double GIC of 13 A and 11 A intensities. This substorm is not apparent in the AL index.

Days 311–312 (6–7 November), 2000 (Fig. A9). This event was previously discussed in Results section (Fig. 5). A constant Bs in a sheath caused a $SYM-H = -176$ nT magnetic storm with peak at ~2104 UT day 311. The strong shock at ~0948 UT (1248 LT) did not cause a GIC above study level threshold. Mäntsälä was in the noon sector at the time of the event.

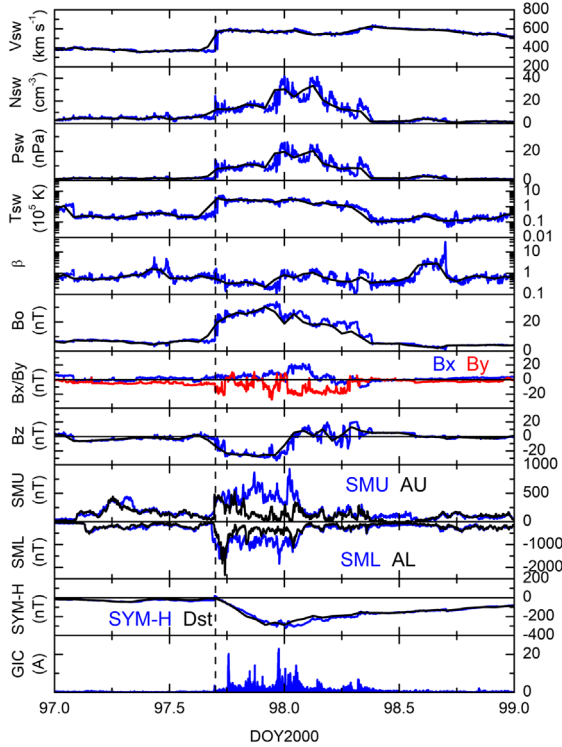


Fig. A4. Events on days 97–98 (6–7 April) 2000. Same format as in Figure A1.

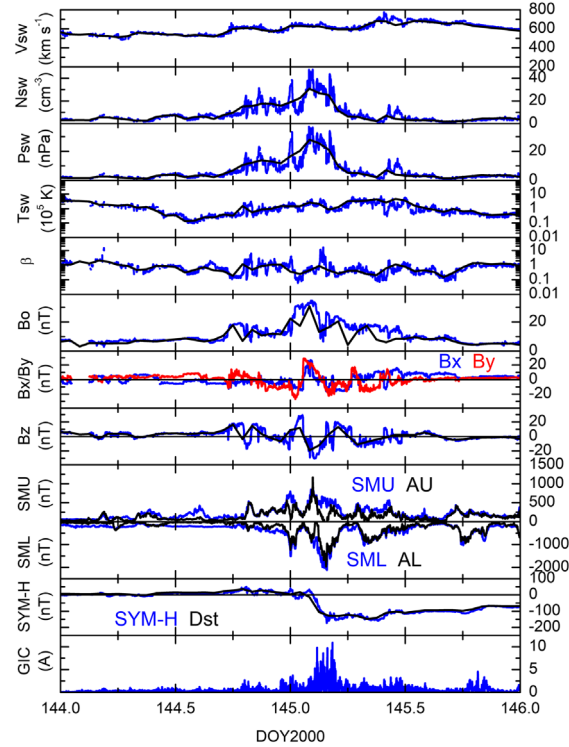


Fig. A5. Events on day 145 (24 May) 2000. Same format as in Figure A1.

A 19 A GIC occurred in the storm main phase with no apparent strong substorm relationship. An unusual sharp short-duration PP of 33 cm^{-3} is related to the GIC. This increased the solar wind ram pressure by a factor of 6.6 times. This PP may be a coronal loop that has propagated to 1 AU.

Day 315 (10 November), 2000 (Fig. A10). A high-speed ($V_{\text{sw}} = 920 \text{ km s}^{-1}$) sheath and intermittent B_s fields caused a $SYM-H = -105 \text{ nT}$ magnetic storm. An interplanetary shock at $\sim 0629 \text{ UT}$ (0929 LT) ahead of an ICME triggers a 10 A GIC spike. Only a moderate intensity substorm was triggered by the shock. Mäntsälä was in the morning sector at the time of the shock. There were no GICs above threshold during the storm main phase. A MC followed the sheath but it had B_n fields and thus leads to the storm recovery phase.

Day 78 (19 March), 2001 (Fig. A11). A double magnetic storm of peak intensity $SYM-H = -164 \text{ nT}$ is caused by a sheath (first dip) and MC (second dip). There is a 16 A GIC in beginning main phase of the storm. The GIC occurred during the decay of a $N_{\text{sw}} = 33 \text{ cm}^{-3}$ solar wind density spike. There is no particularly strong substorm relationship. This GIC event does not have an obvious interplanetary or magnetospheric cause.

Day 90 (31 March), 2001 (Fig. A12). A superstorm of $SYM-H = -437 \text{ nT}$ was caused by sheath fields ahead of an ICME (whose MC B_s caused a second, less intense storm of $SYM-H = -269 \text{ nT}$). The shock at $\sim 0101 \text{ UT}$ (0401 LT) triggered a short-duration substorm of $SML = -1541 \text{ nT}$ and a GIC below threshold. Mäntsälä was in the midnight-dawn sector at the time. Two GICs with $\sim 14 \text{ A}$ intensities occurred in the

initial phase before the storm main phase. These were associated with substorm activity. A 12 A GIC event occurred in the storm main phase. All 3 GIC events were associated with substorm activity. In the second, lesser intensity storm, there are 3 large sharp onset substorms of peak intensities $SML = -2459$, -1721 nT and -1404 nT . The first substorm event caused a 13 A GIC. The second and third substorm-related GICs had intensities of 16 A and 13 A.

Day 101–102 (11–12 April), 2001 (Fig. A13). A shock and sheath with intermittent B_s ahead of a MC caused a superstorm main phase of $SYM-H = -280 \text{ nT}$. The MC begins with intense IMF B_s which may contribute to the peak of the storm main phase. The shock at $\sim 1345 \text{ UT}$ (1645 LT) triggers a SSS of $SML = -2923 \text{ nT}$ intensity but there is no GIC above the 10 A threshold. Mäntsälä was in the afternoon-dusk sector at the time. A GIC of 18 A occurs at the beginning of the storm main phase and occurred in a substorm-intense interval. A 22 A GIC occurred later in the storm main phase and is associated with a substorm $SMU = 1191 \text{ nT}$ peak intensity. This substorm shows up more strongly in SMU rather than SML . A 16 A GIC is noted at the start of the storm recovery phase. This occurred as the substorm activity was subsiding and there was no 1-to-1 relationship with a substorm.

Day 118 (28 April), 2001 (Fig. A14). An ICME event that does not cause a magnetic storm ($SYM-H = -34 \text{ nT}$). The strong shock at $\sim 0502 \text{ UT}$ (0802 LT) caused a SI+ of 75 nT. The shock also triggered a sudden onset substorm of $SML = -498 \text{ nT}$ intensity. The SMU intensity was larger, 777 nT. A 13 A GIC occurred at the same time as the shock and

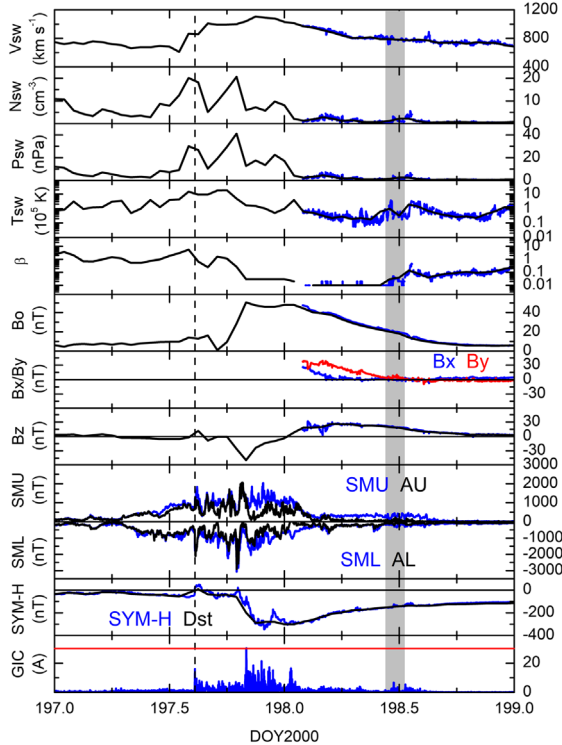


Fig. A6. Events on days 197–198 (15–16 July) 2000. Same format as in [Figure A1](#). The horizontal red line in GIC panel indicates the GIC = 30 A level. The vertical shading represents a ICME filament identified by [Lepri & Zurbuchen \(2010\)](#).

substorm sudden onset. At the time of the shock, Mäntsälä was in the morning sector. There was no intense Bs in the sheath or MC, thus there was no storm.

Day 268–269 (25–26 September), 2001 (Fig. A15). A $SYM-H = -118$ nT magnetic storm caused by a sheath upstream of an ICME. The shock at ~2027 UT (2327 LT) triggered a short-duration substorm of $SML = -1544$ nT intensity and a below threshold GIC event. At the time of the shock Mäntsälä was in the midnight sector. A 20 A GIC was associated with an intense substorm spike of $SML = -2264$ nT occurring in the storm main phase. The intense substorm was caused by a strong solar wind density spike of $N_{sw} = 69 \text{ cm}^{-3}$.

Days 294–295 (21–22 October), 2001 (Fig. A16). An ICME related $SYM-H = -219$ nT magnetic storm. The strong shock at ~1649 UT (1949 LT) created a sudden onset of a $SML = -1148$ nT substorm and a GIC below study threshold. At the time of the shock, Mäntsälä was in the dusk-midnight sector. In the storm main phase, an 11 A GIC is associated with a $SML = -1824$ nT short-duration substorm. A second larger 18 A GIC occurs within a long-duration $SML = -1160$ nT substorm. Both the latter GIC and substorm onset occur at the same time as a $N_{sw} = 65 \text{ cm}^{-3}$ solar wind density spike. This occurred in the storm recovery phase. Two more GICs of 12 A and 13 A intensity occur in a multiple substorm period. There is no obvious 1-to-1 relationship between the GICs and the substorms for these two GIC events. A ICME filament is indicated by the vertical shading at ~1200 UT day 295. There are some small

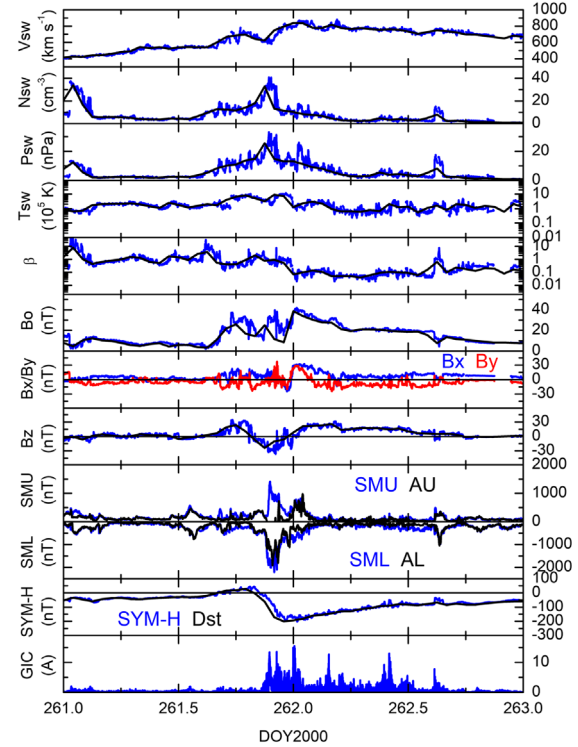


Fig. A7. Events on days 261–262 (17–18 September) 2000. Same format as in [Figure A1](#).

GICs present during the interval but they are below the study threshold.

Day 310 (6 November), 2001 (Fig. A17). The sheath portion of an ICME (there is a data gap) causes a $SYM-H = -320$ nT superstorm. Although the shock occurred in a data gap, a clear SI^+ of intensity 86 nT at ~0153 UT (0453 LT) and a correlated 32 A GIC were present. Mäntsälä was in the dawn sector. The shock triggered a short-duration $SML = -2301$ nT intense substorm. There were intense $SML = \sim -2300$ nT substorm activities (following the initial intense substorm) with many GIC events with intensities up to 27 A. In the storm recovery phase two SSSs of even greater intensities of $SML = -2839$ nT and -2494 nT occurred, but these did not cause GICs above the study threshold.

Day 328 (24 November), 2001 (Fig. A18). A sheath upstream of an ICME caused a double dip magnetic storm of $SYM-H = -233$ nT peak intensity. The MC had a northward IMF orientation and caused the recovery phase of the storm. The shock occurred at ~0600 UT (0900 LT), when Mäntsälä was in the morning sector. The shock triggered a long-duration SSS which peaked at $SML = -3839$ nT hours later. Either the shock or the onset of the SSS caused a 21 A GIC. The SSS peak was correlated with a 32 A GIC. Later GICs of 25 A and 26 A were associated with the decay phase of the SSS. The SSS was triggered/enhanced in intensity by a $N_{sw} = 65 \text{ cm}^{-3}$ (PP) and an IMF B_n turning. The PP may be a coronal loop portion of the ICME. In the second dip of the storm, another SSS of $SML = -3281$ nT peak intensity caused GICs of 12, 10 and 11 A. There were 40 >10 A GICs in this day.

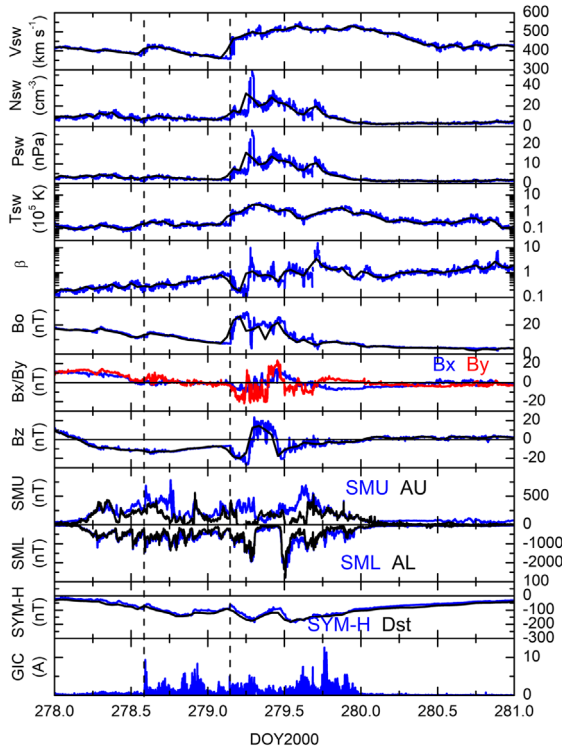


Fig. A8. Events on days 278–279 (4–5 October) 2000. Same format as in [Figure A1](#).

Day 107 (17 April), 2002 ([Fig. A19](#)). A storm of $SYM-H = -100$ nT is caused by the sheath ahead of an ICME. The shock at ~1107 UT (1407 LT) was time-coincident with a GIC of 19 A and a $SML = -1523$ nT sharp onset substorm. Mäntsälä was in the afternoon sector at the time of the shock. There were no GICs of threshold intensities during the storm main phase.

Day 143 (May 23), 2002 ([Fig. A20](#)). A double dip magnetic storm with peak intensity $SYM-H = -115$ nT was caused by a compound interplanetary event: shock/sheath, MC, and a possible filament. A B_s field in the MC caused the first storm dip and the following B_s interval at the onset of the high-density possible filament (35 cm^{-3}) at ~1546 UT (1846 LT), indicated by the vertical red dashed line, caused the second storm dip. The shock at ~1051 UT (1351 LT) created a $SML = -662$ nT substorm and a 10 A GIC. The substorm is not detected in the AL index nor the SML indices. It is noted by the SMU index alone ($SMU = 1726$ nT). Mäntsälä was in the afternoon sector during this event. The filament B_s caused the second dip of the storm. The possible filament and its B_s triggered a $SML = -1760$ nT long-duration substorm and many GICs, but not above the 10 A threshold of this study. It is possible that this substorm caused the second dip of the two-dip storm.

Days 250–251 (7–8 September), 2002 ([Fig. A21](#)). A double dip storm with peak intensity $SYM-H = -168$ nT was caused by sheath B_s variations ahead of a MC. The shock at ~1637 UT (1937 LT) created a GIC but below the threshold of this study. Mäntsälä was in the dusk sector at the time. There were three clear GICs of 26, 21 and 24 A intensities. The first GIC is correlated with an IMF B_n turning ending the first dip storm. The B_n turning started the recovery of the first dip storm. There was

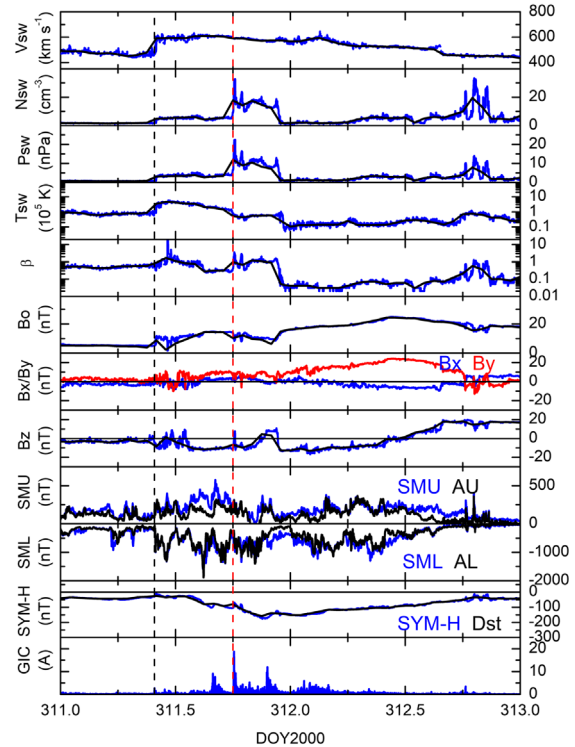


Fig. A9. Events on days 311–312 (6–7 November) 2000. Same format as in [Figure A1](#). The vertical red dashed line indicates a PP event.

no substorm associated with the GIC. The second GIC had no obvious substorm or interplanetary related features. The third GIC occurred in the beginning of the storm recovery phase and was associated with a substorm of $SML = -1116$ nT intensity.

Days 274–275 (1–2 October), 2002 ([Fig. A22](#)). This event was previously discussed in Results section ([Fig. 8](#)). A low-speed solar wind at $V_{sw} \sim 420 \text{ km s}^{-1}$ with a long-period B_z wave with B_s reaching ~23 nT caused a $SYM-H = -153$ nT magnetic storm (peak at ~1253 UT day 274). There was geomagnetic auroral zone activity in this low-speed solar wind. A $SML = -1906$ nT short-duration substorm spike caused a double GIC of 28 A and 19 A intensities. The GICs occurred in the beginning of the storm recovery phase. There is no obvious interplanetary cause of this substorm.

Day 297 (24 October), 2002 ([Fig. A23](#)). A high-speed stream of $V_{sw} \sim 800 \text{ km s}^{-1}$ peak speed caused a CIR and HILDCAA-like interval. The B_s in the CIR caused a day-long $SYM-H = -88$ nT magnetic storm. There were no shocks. The CIR double B_s feature caused two long-duration substorms with peak intensities of $SML = -1306$ nT and -1112 nT. Neither substorm caused a GIC of intensity over the study level. A double GIC of 19 A and 14 A were associated with a much smaller substorm of $SML = -993$ nT intensity.

Days 149–150 (29–30 May), 2003 ([Fig. A24](#)). A double shock/sheath event. The second sheath B_s caused a $SYM-H = -164$ nT magnetic storm. The MC had a B_n field and caused the storm recovery phase. The first shock at ~1226 UT

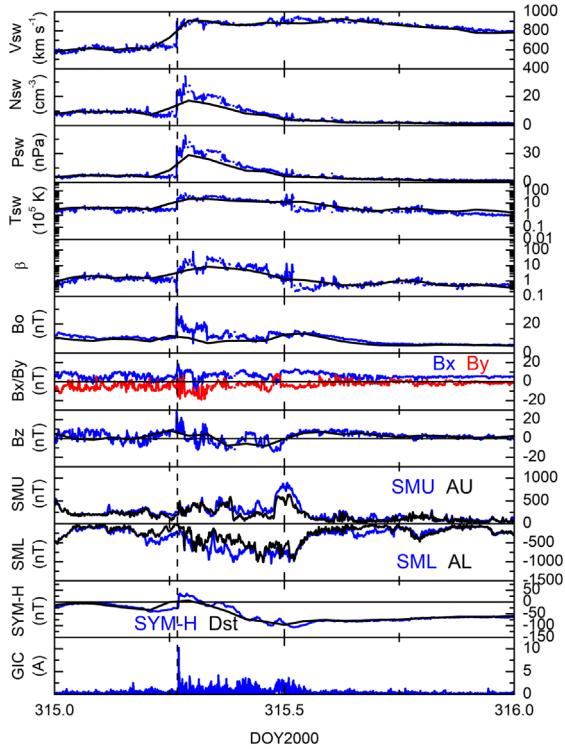


Fig. A10. Events on day 315 (10 November) 2000. Same format as in Figure A1.

(1526 LT) did not trigger a substorm nor a GIC of study level intensity. The second shock occurred at 1913 UT (2213 LT) and triggered an intense substorm of *SML* intensity -2461 nT. The shock-related GIC did not reach the study threshold. Mäntsälä was in the afternoon sector during the first shock and in the dusk-midnight sector during the second shock. A cluster of GICs with peaks of 11 A, 11 A, 11 A and 12 A occurred in the storm main phase but there are no obvious 1-to-1 correlations with substorm peaks.

Day 287 (14 October), 2003 (Fig. A25). CIR Bs fields caused a double dip magnetic storm of *SYM-H* = -103 nT intensity. There was no shock. The CIR double dip wave in *Bz* causing two long-duration substorms with peak intensities of *SML* = -1447 nT and -1385 nT. The two substorms caused the double dip magnetic storm. The first substorm peak causes a GIC of 29 A. The second substorm caused GICs, but below the study threshold. The high-speed stream proper had a peak speed of 750 km s^{-1} .

Days 302–303 (29–30 October), 2003 (Fig. A26). This event was previously discussed in Results section (Fig. 2). A sheath and MC Bs caused the first October Halloween super-storm of intensity *SYM-H* = -390 nT. This was a double dip magnetic storm with the sheath causing the first dip and a MC Bs causing the second dip. The strong shock at ~ 0612 UT (0912 LT) and triggered the sharp onset of a long duration, two-peak SSS of *SML* = -3177 nT (at 0624 UT) and -3548 nT (at 0648 UT) intensity and a cluster of GICs of 33 A (at 0646 UT), 57 A (at 0657 UT), 51 A (at 0703 UT) and 52 A (at 0727 UT) later in the event. Either the shock or the onset of the SSS caused a GIC of 25 A. Mäntsälä was in the morning sector at

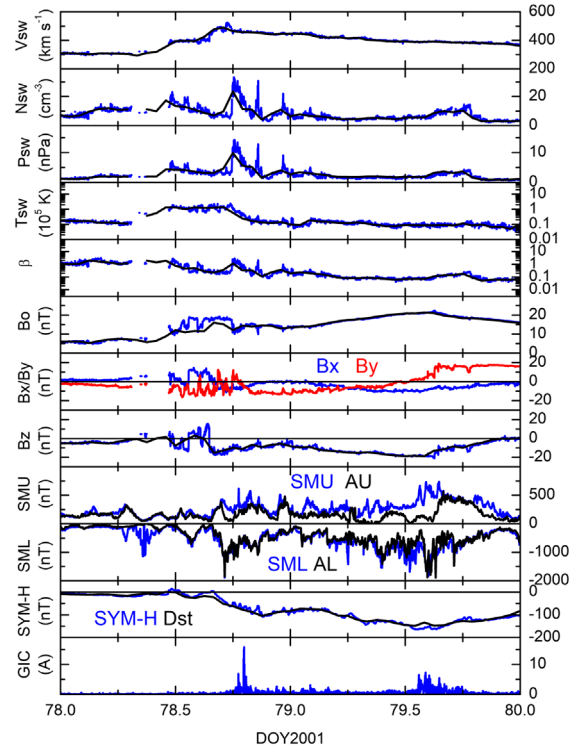


Fig. A11. Events on day 78 (19 March) 2001. Same format as in Figure A1.

the time of the largest GICs. There are many GICs > 10 A in the two main phases of this double dip storm. However, the most intense events occurred in the first SSS immediately after the shock. There is a GIC of 30 A at 2230 UT (0130 LT) day 302 at the start of the second dip storm. This is associated with an intense storm of *SML* = -2340 nT. There is a 36 A GIC at 0110 UT (0410 LT) day 303 at the start of the recovery phase of the second dip storm.

Days 303–304 (30–31 October), 2003 (Fig. A27). This event was previously discussed in Results section (Fig. 3). The second “Halloween” superstorm. A sheath Bs upstream of an ICME causes the second October Halloween storm of intensity *SYM-H* = -432 nT. A solar wind density spike (PP) at ~ 1949 UT (2249 LT) (denoted by the SI^+ of ~ 61 nT) created a GIC of 49 A and a short-duration SSS of amplitude *SML* = -3872 nT. Mäntsälä was in the midnight sector at the time. A second short-duration *SML* = -2724 nT SSS occurred in the storm main phase. It is associated with a double GIC of 33 and 27 A. There are two clusters of GICs with > 10 A intensities in the storm recovery phase. They are associated with sub-storm intervals of peak intensities of *SML* = -1821 and -797 nT, respectively. In the first cluster there is a GIC of 30 A at 0213 UT on day 304. In the second cluster there is a 27 A GIC at 0536 UT day 304. There is a fourth GIC cluster with 16 A at 1119 UT, 19 A at 1152 UT, 16 A at 1119 UT, 14 A at 1227 UT and 16 A at 1246 UT. There were 90 GICs > 10 A and 3 GICs > 30 A.

Days 324–325 (20–21 November), 2003 (Fig. A28). The third “Halloween” superstorm. The November 2003 Halloween storm of *SYM-H* = -490 nT intensity was caused by Bs in the

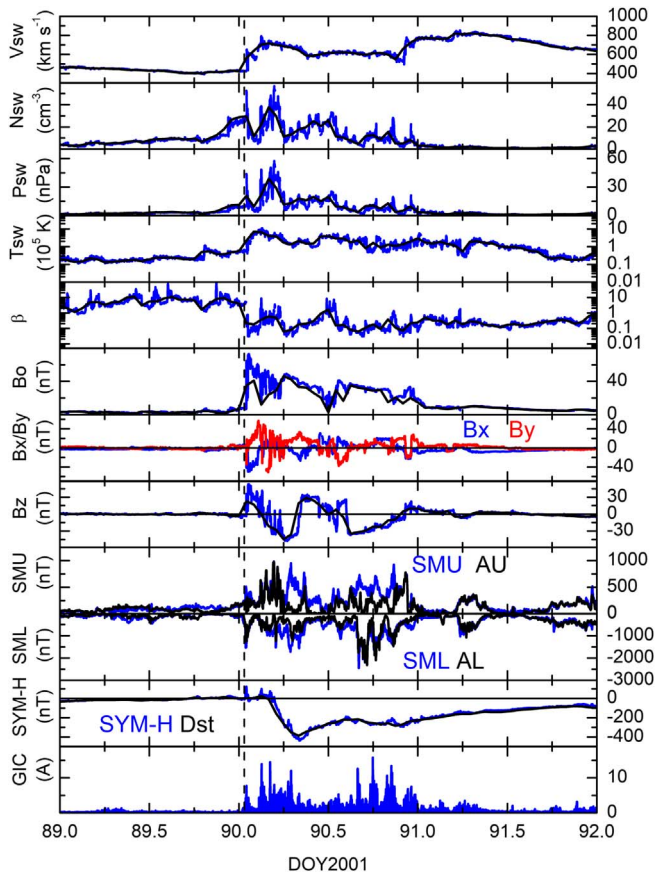


Fig. A12. Events on day 90 (31 March) 2001. Same format as in Figure A1.

sheath, Bs in an ICME MC followed by a possible filament. The shock at ~0803 UT (1103 LT) only created a small GIC below the study threshold and a *SML* = −2031 nT short-duration sharp onset intense substorm. Mäntsälä was in the noon sector at the time of the shock. In the MC generated storm main phase, there are 4 large GICs. A short-duration substorm detected only in *SMU* (912 nT) is coincident with the first GIC of 23 A at 1408 UT. The next two GICs of 19 A (at 1518 UT) and 24 A (at 1640 UT) are not related to any obvious substorm features. A SSS of *SML* = −4141 nT intensity at 1634 UT caused the largest (double) GIC of 19 A and 24 A. These may be associated with a sharp solar wind density spike of 25 cm^{-3} . The density spike is the onset of a possible ICME filament. There is a 16 A GIC in the storm recovery phase caused by the last, isolated substorm of amplitude *SML* = −1714 nT.

Day 326 (22 November), 2003 (Fig. A29). This interval was a HSS with a relatively constant $V_{\text{sw}} \sim 540\text{--}640 \text{ km s}^{-1}$ speed. The IMF Bs peak of −9.2 nT generated a magnetic storm of *SYM-H* = −97 nT. There was no obvious shock and/or CIR. In the first Bs interval there is a cluster of substorms with *SML* peaks all of ~ 1500 nT intensities. One large GIC of 14 A is associated with one short-duration substorm of intensity *SML* = −1561 nT. This substorm cannot be detected in the *AL* index. It is most remarkable in the *SMU* index. The other substorms with the same intensities did not generate GICs above the study threshold.

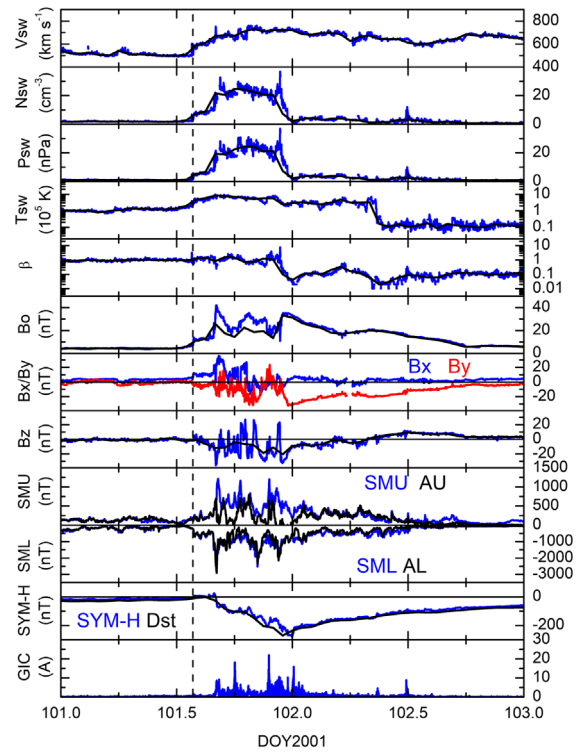


Fig. A13. Events on days 101–102 (11–12 April) 2001. Same format as in Figure A1.

Day 344 (10 December), 2003 (Fig. A30). A pure HSS event with a peak speed of $V_{\text{sw}} = 840 \text{ km s}^{-1}$ caused a magnetic storm of *SYM-H* = −71 nT intensity. Alfvénic Bs fluctuations caused a HILDCAA interval with lots of substorms, but no SSSs. One isolated 11 A GIC is caused by a substorm with *SML* peak intensity of −1830 nT. This substorm is not detected in the *AL* index.

Day 94 (3 April), 2004 (Fig. A31). A moderate speed ICME whose upstream sheath/pileup region caused a double dip magnetic storm of *SYM-H* = −149 nT intensity. The peak speed of the ICME is only $\sim 496 \text{ km s}^{-1}$ in a background $V_{\text{sw}} \sim 400 \text{ km s}^{-1}$. The storm double dip is caused by a long B_z wave giving 2 intervals of Bs in the sheath ahead of the MC. The MC has a B_n field and leads to the storm recovery phase. The shock at ~1413 UT (1713 LT) did not cause a GIC with intensity above study level. At the time Mäntsälä was in the dusk sector. One GIC of 11 A occurred at the cusp between the first dip storm and the second dip storm. There was no obvious substorm or solar wind feature associated with this GIC.

Days 312–313 (7–8 November), 2004 (Fig. A32). A triple dip *SYM-H* = −382 nT superstorm caused by a sheath Bs interval and a MC Bs interval. There were three shocks and sheaths in this interplanetary event but the first two shocks were not geoeffective. Both the first shock at the beginning of day 312 and the second shock at ~1056 UT (1356 LT) day 312 created below threshold GIC events. The third shock at ~1829 UT (2129 LT) was time-coincident with a 11 A GIC event. Mäntsälä was in the dusk sector during the second shock and in the dusk-midnight sector during the third shock. There are

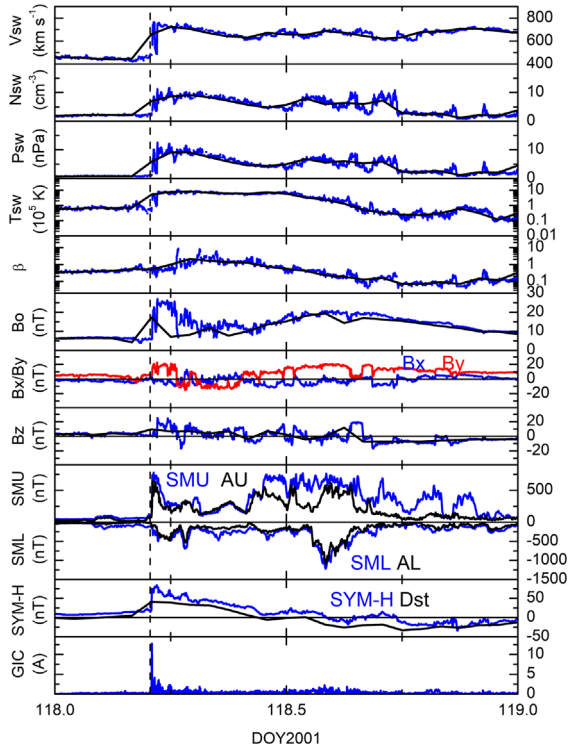


Fig. A14. Events on day 118 (28 April) 2001. Same format as in Figure A1.

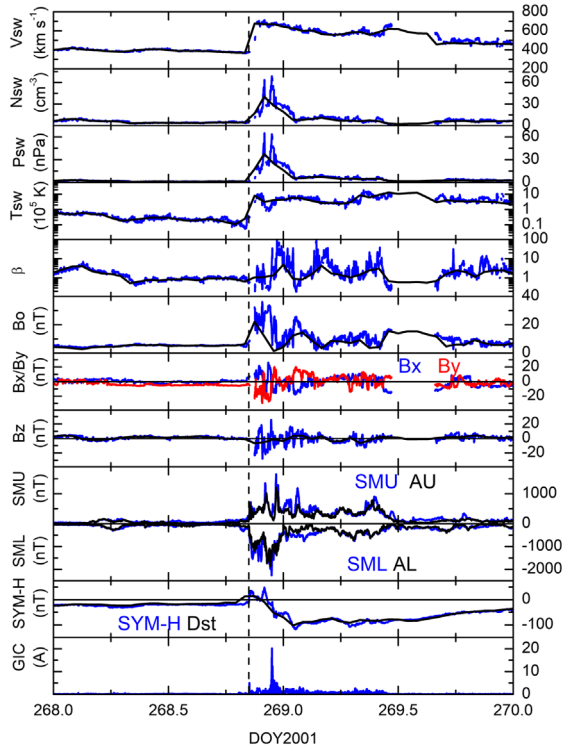


Fig. A15. Events on days 268–269 (25–26 September) 2001. Same format as in Figure A1.

two GIC event clusters occurring in the storm main phase. The largest GIC event of 35 A occurred in the first cluster during an intense substorm of *SML* amplitude -2071 nT. The intense substorm was triggered by a solar wind PP and a sharp Bs intensification. The PP had a peak density of ~ 29 cm⁻³. It could possibly a loop portion of the ICME. The second GIC cluster had many GICs > 10 A (peak of ~ 29 A) and occurred near third dip storm maximum. These individual GICs within the clusters do not appear to have one-to-one associations with substorm peak intensities. The GICs appear to be terminated by a reverse shock which decreased the IMF Bs. There were 38 > 10 A GIC events during these two days.

Day 314 (9 November), 2004 (Fig. A33). A shock/sheath, shock/sheath and MC compound event causing a triple dip superstorm with intensities of -139 nT, -271 nT and -282 nT, respectively. The first dip storm is caused by the first sheath Bs, the second dip storm by the second sheath Bs and the third storm by the MC Bs. The first shock at ~ 0932 UT (1232 LT) triggered a GIC below the study threshold. The second shock at ~ 1850 UT (2150 LT) also did not trigger a GIC above the study threshold. At the time of these two shocks, Mäntsälä was in the noon sector and dusk-midnight sectors, respectively. The second shock triggered an intense substorm which reached a peak value of *SML* = -2264 nT hours later. The substorm was due to sheath Bs which caused the second dip storm main phase. The second storm has a peak intensity of *SYM-H* = 271 nT at 2103 UT day 314. This substorm onset is caused by a sharp Bs intensification associated with the shock compression of preexisting Bs fields. This intense substorm caused a

cluster of three GICs with 43, 42 and 21 A intensities. There were 20 GIC > 10 A intensities during this day.

Day 21 (21 January), 2005 (Fig. A34). This event was previously discussed in Results section (Fig. 6). An ICME preceded by a strong shock/sheath. The sheath caused a storm of *SYM-H* = -101 nT. The shock at ~ 1712 UT (2012 LT) was time-coincident with a GIC of 13 A and triggered a sharp onset of a *SSS* which reached a peak value of *SML* = -4418 nT. Mäntsälä was in the dusk-midnight sector at the time. During the *SSS* decay phase there is a cluster of GICs reaching 27 A. The GICs and substorm *SMU* intensification are associated with an unusual sharp interplanetary density spike up to *Nsw* = 55 cm⁻³. There is another GIC of intensity 22 A at 2015 UT which is time-coincident with a sharp solar wind density spike to 42 cm⁻³. There is no obvious substorm feature associated with this GIC. There were 12 GICs with > 10 A in this event.

Day 236 (24 August), 2005 (Fig. A35). A shock/sheath event ahead of an ICME event where the sheath Bs causes a magnetic storm of intensity *SYM-H* = -179 nT. The shock at ~ 0614 UT (0914 LT) caused a GIC below the study threshold. Mäntsälä was in the morning sector at the time of the shock. In the storm main phase there are two *SSS*s with *SML* = -4046 nT and -3895 nT peak intensities. There are no GICs above threshold associated with these events. There is a cluster of GICs with peak intensity of 13 A that occur in the *SSS* decay phase. This is at the end of the storm main phase and beginning of the recovery phase. There is no 1-to-1 correlation with the substorms.

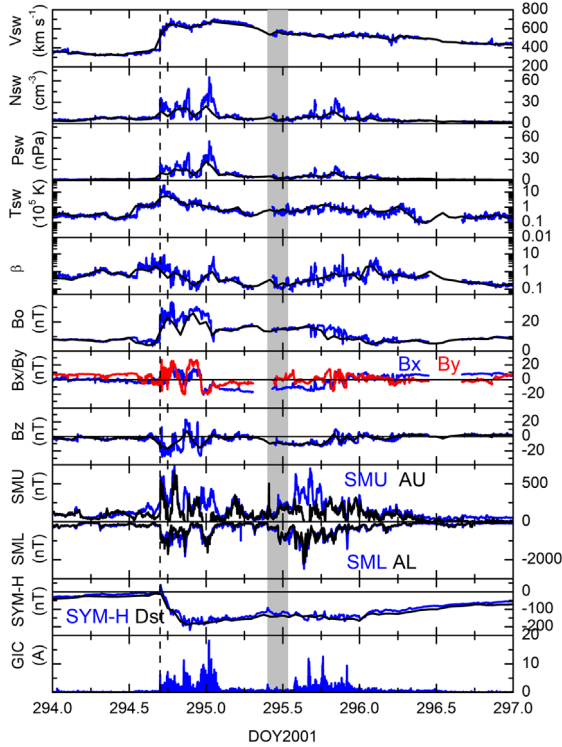


Fig. A16. Events on days 294–295 (21–22 October) 2001. Same format as in Figure A1. A ICME filament identified by Lepri & Zurbuchen (2010) is indicated by the vertical shading.

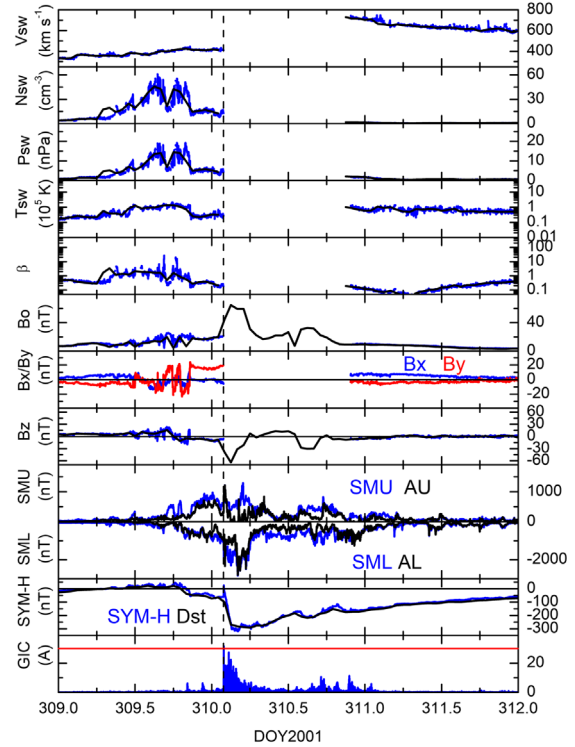


Fig. A17. Events on day 310 (6 November) 2001. Same format as in Figure A1.

Day 349 (15 December), 2006 (Fig. A36). An ICME event where the MC Bs caused a storm of $SYM-H = -220$ nT intensity. The strong shock at ~1414 UT (1714 LT) triggered an intense substorm of $SML = -2102$ nT intensity. Due to a GIC data gap, it is unknown whether there a GIC above study threshold or not. In the storm main phase there is an intense substorm of $SML = -2264$ nT. A GIC of 14 A at 0055 UT is associated with the decay part of this substorm. There were three more GICs with > 10 A intensities. They occurred at 0148 UT, 0224 UT and 0518 UT and have intensities of 13 A, 11 A and 12 A, respectively. There are no obvious 1-to-1 GIC relationships with substorms.

Day 269 (26 September), 2011 (Fig. A37). A CIR and HSS event (maximum speed of $V_{sw} = 734$ km s $^{-1}$) where the CIR Bs causes a storm of intensity $SYM-H = -116$ nT. The shock at ~1236 UT (1536 LT) triggers a short-duration substorm of intensity $SML = -866$ nT but no GIC above study level. Mäntsälä was in the afternoon sector at the time of the shock. Two GICs of 12 and 16 A occurred in the storm main phase, but there are not obviously 1-to-1 associated with substorms. The first GIC occurs in the decay phase of an intense substorm of $SML = -2006$ nT and the second more intense event occurs when the SML level is < -500 nT ($SML = -300$ nT). The latter GIC is due to a solar wind plasma density spike. There is no associated substorm.

Day 58 (27 February), 2012 (Fig. A38). This event was previously discussed in Results section (Fig. 7). A $V_{sw} \sim 520$ km s $^{-1}$ slow ICME with no shock where the pileup Bs

fluctuations lead to a storm of $SYM-H = -61$ nT. The MC $B_z = 0$ nT causes the storm recovery phase. In this pileup region, there are moderate SML values with a peak of -848 nT but no intense GICs. A GIC event of 20 A is associated with an IMF B_n turning at the sheath/MC boundary. There is also a solar wind ram pressure decrease at that time. There are no substorms or GICs associated with the MC interval with IMF B_n . A high plasma density region of 17.5 cm $^{-3}$ follows the MC. This may be an ICME filament. The density causes a Bs interval and a substorm of $SML = -1142$ nT at 0736 UT (1036 LT) on day 59. The substorm only creates below threshold GICs.

Day 75 (15 March), 2012 (Fig. A39). The sheath Bs upstream of an ICME causes a magnetic storm of $SYM-H = -79$ nT. The MC $B_z = 0$ nT leads to the storm recovery phase. The shock at 1307 UT (1607 LT) causes a GIC below the study threshold. Mäntsälä was in the afternoon sector at that time. A GIC of 39 A occurs at 1703 UT (2003 LT) on day 75 in main phase of the magnetic storm. There is a solar wind spike of density 12 cm $^{-3}$ at 1704 UT that is the cause of the GIC.

Day 76 (17 March), 2013 (Fig. A40). An upstream sheath double Bs event caused a $SYM-H = -131$ nT double dip magnetic storm. The shock at ~0601 UT (0901 LT) triggered a $SML = -958$ nT substorm but no GIC above the study limit. Mäntsälä was in the morning sector at the time of the shock. There is a cluster of 3 GICs of 32, 20 and 14 A intensities in the storm main phase near the storm peak. The GICs occurred on the decay phase of the substorm when the SML intensity was ~ -990 nT. There were no obvious one-to-one relationships

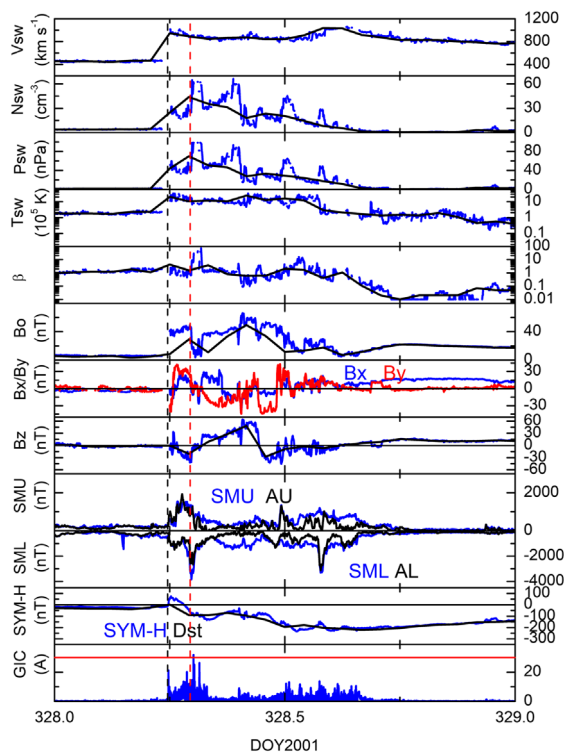


Fig. A18. Events on day 328 (24 November) 2001. Same format as in Figure A1. The GIC = 30 A level is shown by the horizontal red line in the GIC panel. The vertical red dashed line indicates a PP incidence.

between the GICs and substorm features. There were 7 GIC events with >10 A in this day.

Day 275 (2 October), 2013 (Fig. A41). A magnetic storm of intensity $SYM-H = -90$ nT caused by sheath Bs fields. The shock at ~ 0156 UT (0456 LT) triggered a moderate intensity substorm and no GIC above the study limit. The sheath Bs fields caused two substorms, the first of $SML = -2017$ nT and a second of $SML = -1963$ nT. The substorms caused the storm main phase. The first substorm did not cause a GIC above the study limit. The second substorm causes a GIC of 15 A intensity.

Day 254 (11 September), 2015 (Fig. A42). A small $V_{sw} = \sim 640$ km s $^{-1}$ HSS, with presumably Bs (there is a data gap) that causes a $SYM-H = -94$ nT double dip storm. A GIC double event of 16 A occurred in an interplanetary data gap at the start of the storm recovery phase. The GIC occurs at the end of substorm activity in the recovery phase of a $SML = -1014$ nT substorm.

Day 280 (7 October), 2015 (Fig. A43). This is a double dip storm with intensities of $SYM-H = -88$ nT and -124 nT. The first storm was caused by small Bs in a $V_{sw} \sim 460$ km s $^{-1}$ slow solar wind. There were no major GICs associated with this event. The second storm is caused by CIR Bs (with no forward shock) ahead of a HSS of ~ 650 km s $^{-1}$. There were two small clusters of GICs. The first had a peak intensity of 21 A and was associated with a substorm of $SML = -1573$ nT intensity. The second cluster reached 17 A and were not associated with

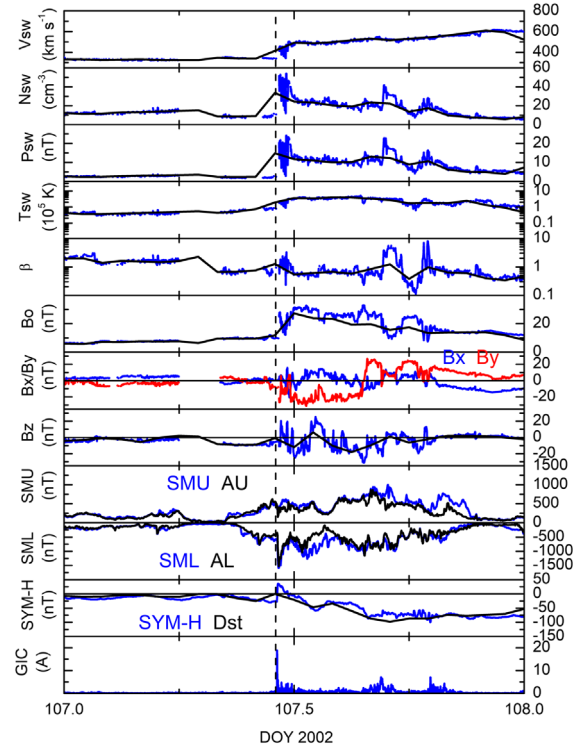


Fig. A19. Events on day 107 (17 April) 2002. Same format as in Figure A1.

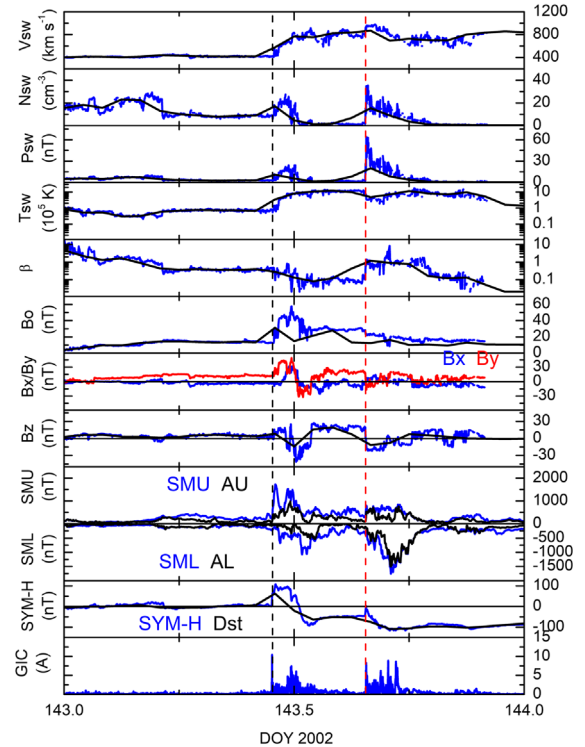


Fig. A20. Events on day 143 (23 May) 2002. Same format as in Figure A1. The vertical red dashed line indicates a possible filament.

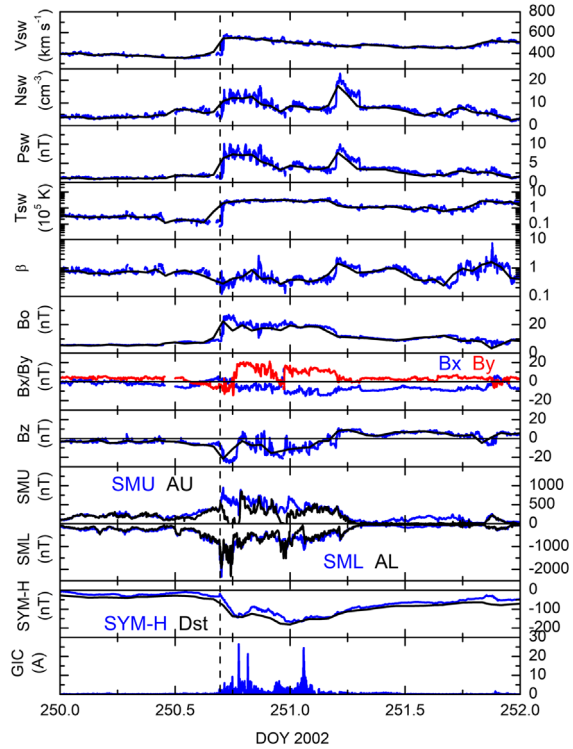


Fig. A21. Events on days 250–251 (7–8 September) 2002. Same format as in Figure A1.

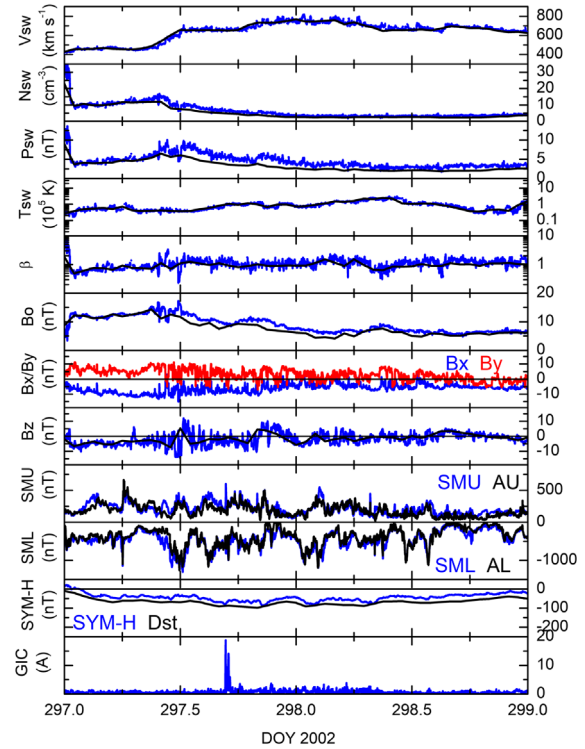


Fig. A23. Events on day 297 (24 October) 2002. Same format as in Figure A1.

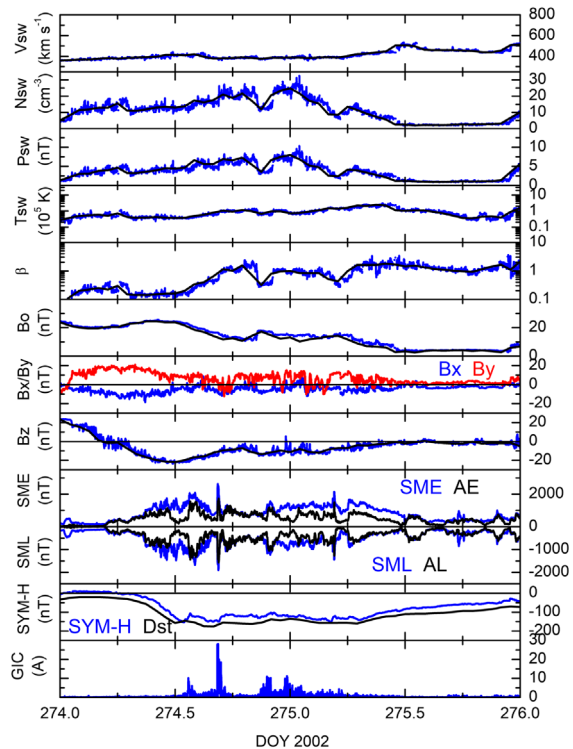


Fig. A22. Events on days 274–275 (1–2 October) 2002. Same format as in Figure A1.

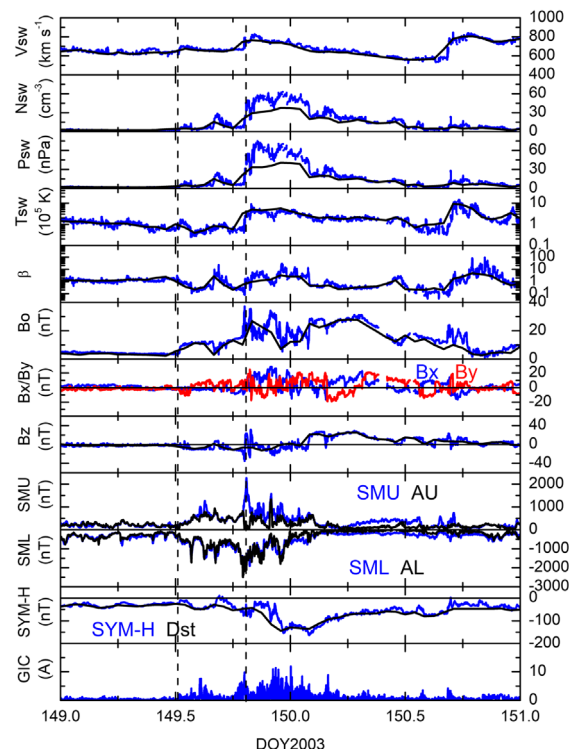


Fig. A24. Events on days 149–150 (29–30 May) 2003. Same format as in Figure A1.

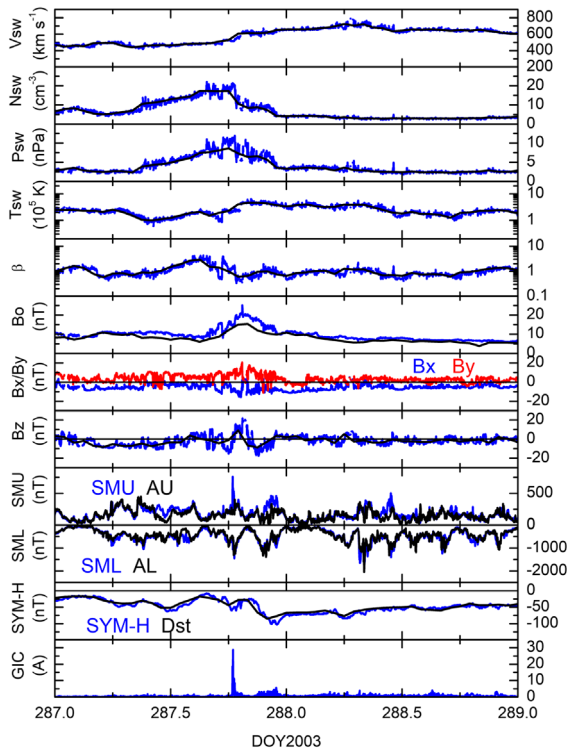


Fig. A25. Events on day 287 (14 October) 2003. Same format as in Figure A1.

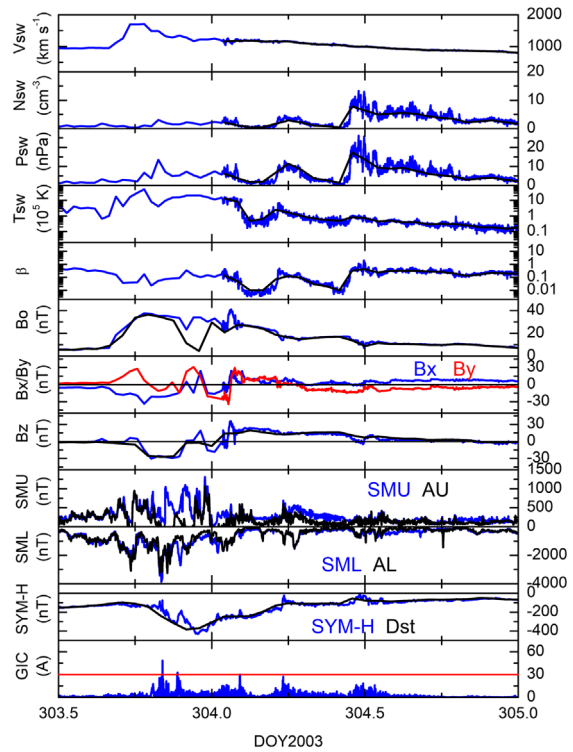


Fig. A27. Events on days 303–304 (30–31 October) 2003. Same format as in Figure A1. The red horizontal line in the GIC panel indicates the GIC = 30 A level.

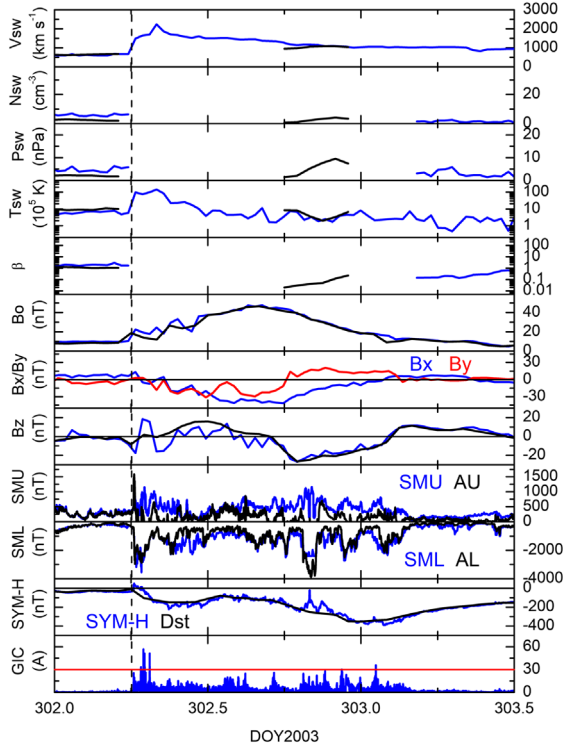


Fig. A26. Events on days 302–303 (29–30 October) 2003. Same format as in Figure A1. The red horizontal line in the GIC panel indicates the GIC = 30 A level.

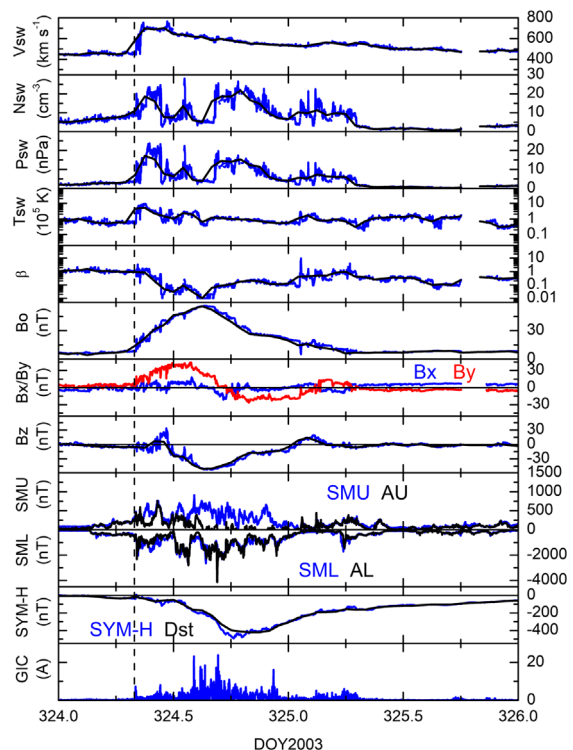


Fig. A28. Events on days 324–325 (20–21 November) 2003. Same format as in Figure A1.

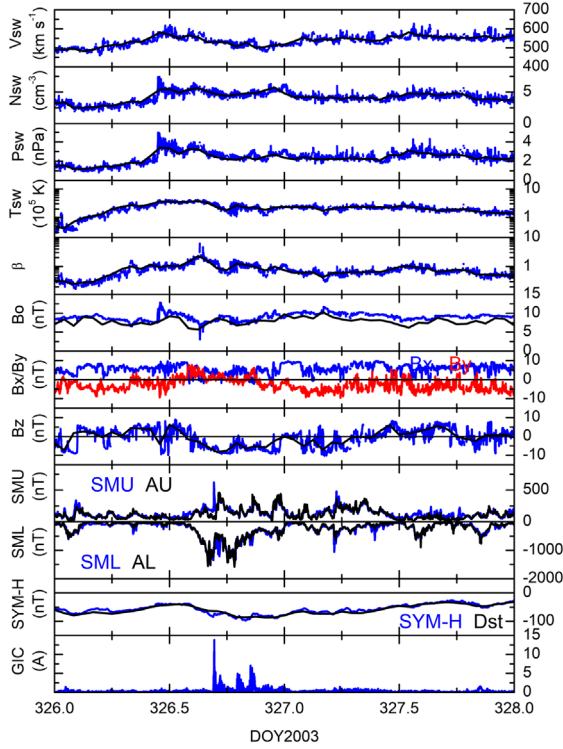


Fig. A29. Events on day 326 (22 November) 2003. Same format as in Figure A1.

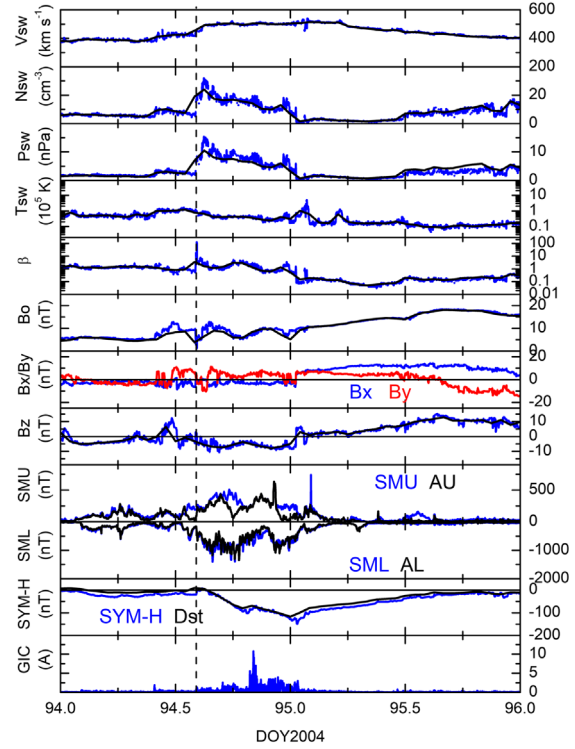


Fig. A31. Events on day 94 (3 April) 2004. Same format as in Figure A1.

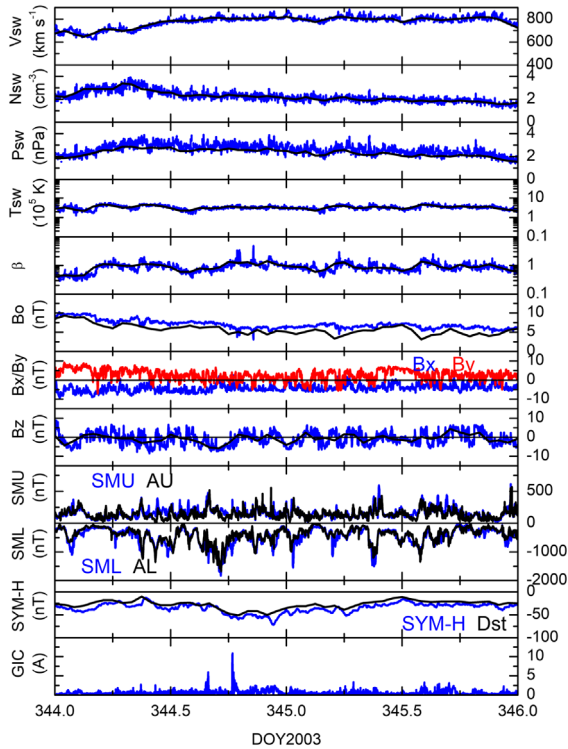


Fig. A30. Events on day 344 (10 December) 2003. Same format as in Figure A1.

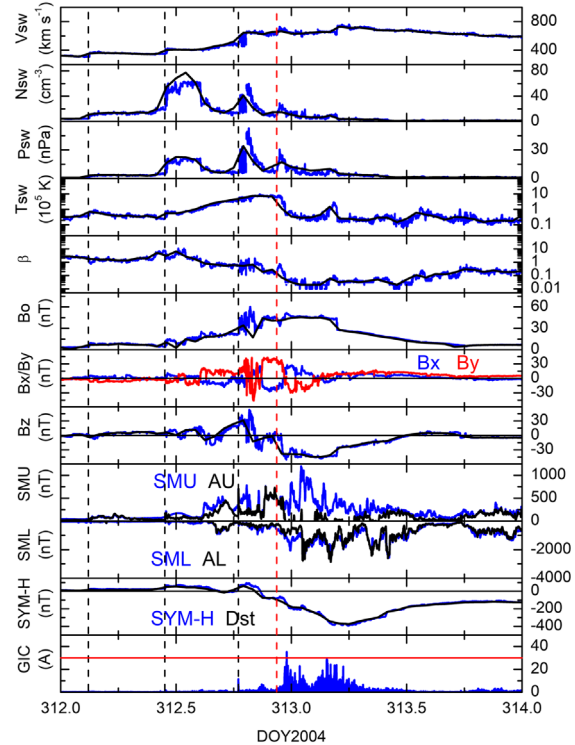


Fig. A32. Events on days 312–313 (7–8 November) 2004. Same format as in Figure A1. The horizontal red line in the GIC panel indicates the GIC = 30 A level. The vertical red dashed line indicates a PP incidence.

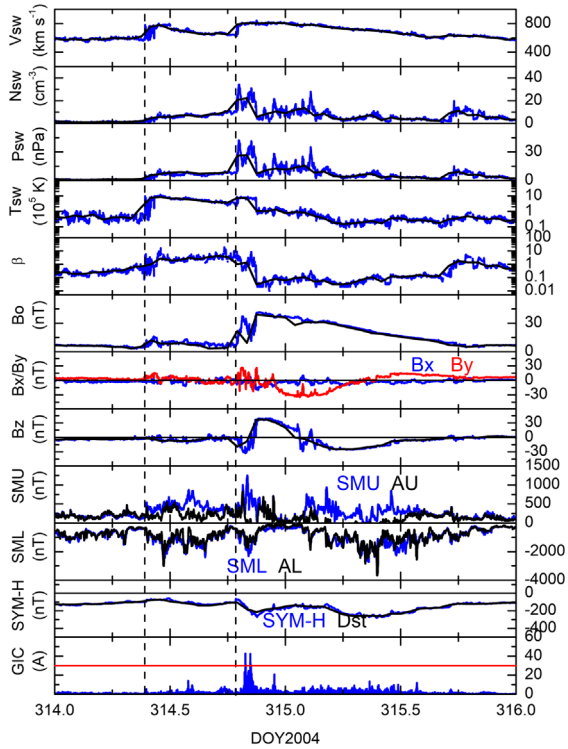


Fig. A33. Fig. A33. Events on day 314 (9 November) 2004. Same format as in Figure A1. The horizontal red line indicates the GIC = 30 A level.

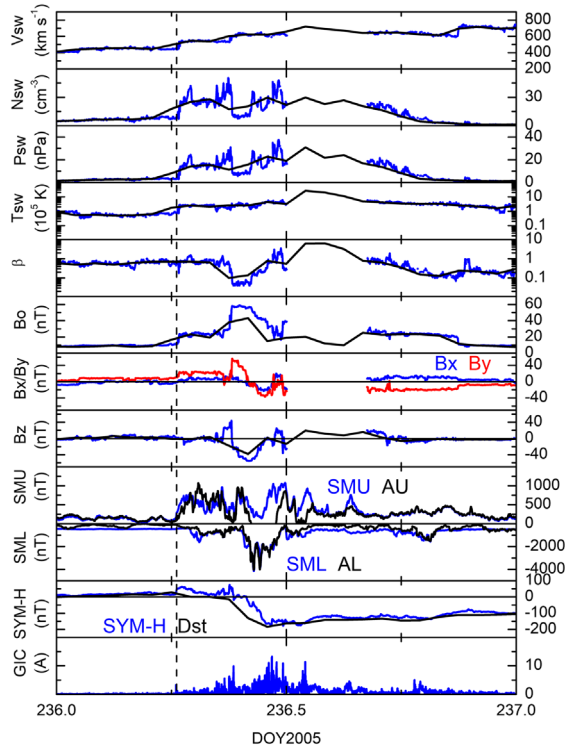


Fig. A35. Events on day 236 (24 August) 2005. Same format as in Figure A1.

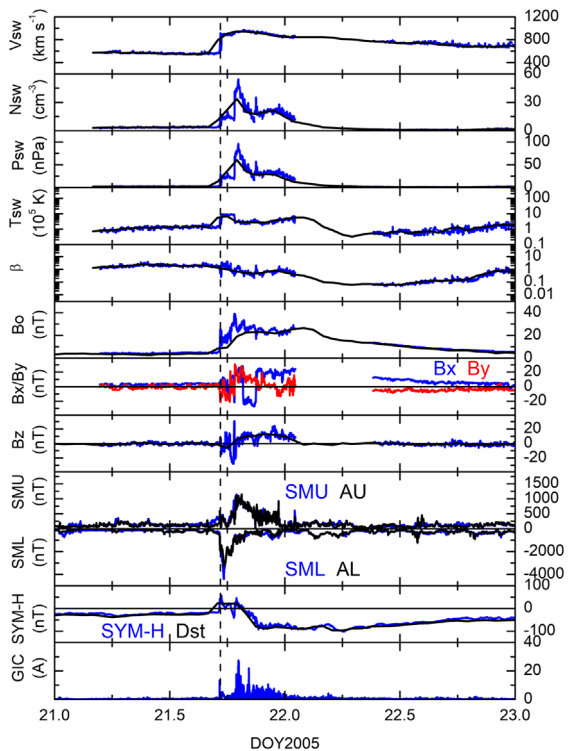


Fig. A34. Events on day 21 (21 January) 2005. Same format as in Figure A1.

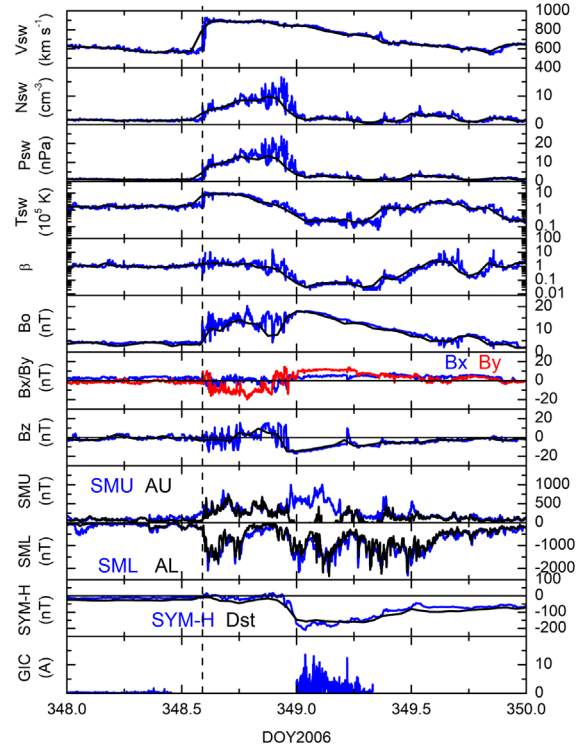


Fig. A36. Events on day 349 (15 December) 2006. Same format as in Figure A1.

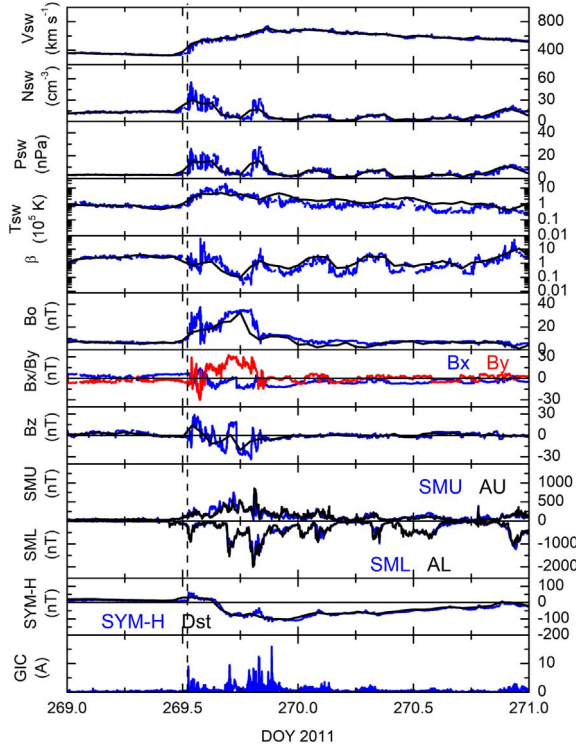


Fig. A37. Events on day 269 (26 September) 2011. Same format as in Figure A1.

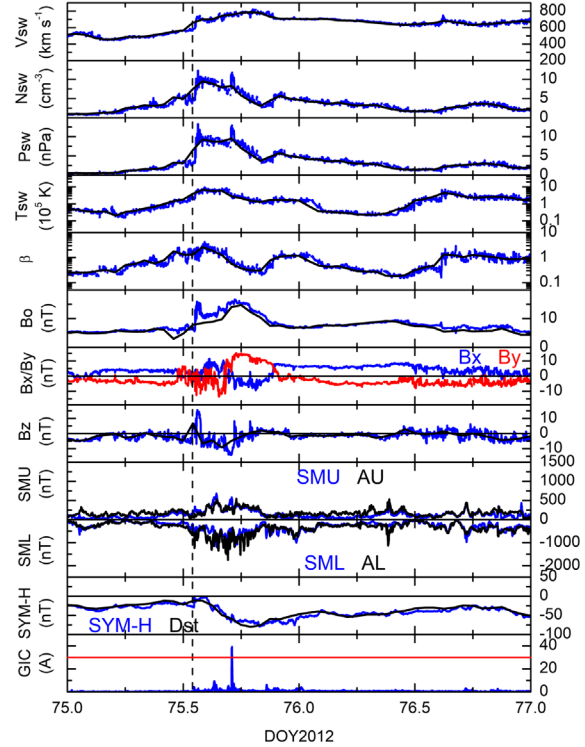


Fig. A39. Events on day 75 (15 March) 2012. Same format as in Figure A1. The horizontal red line indicates the GIC = 30 A level.

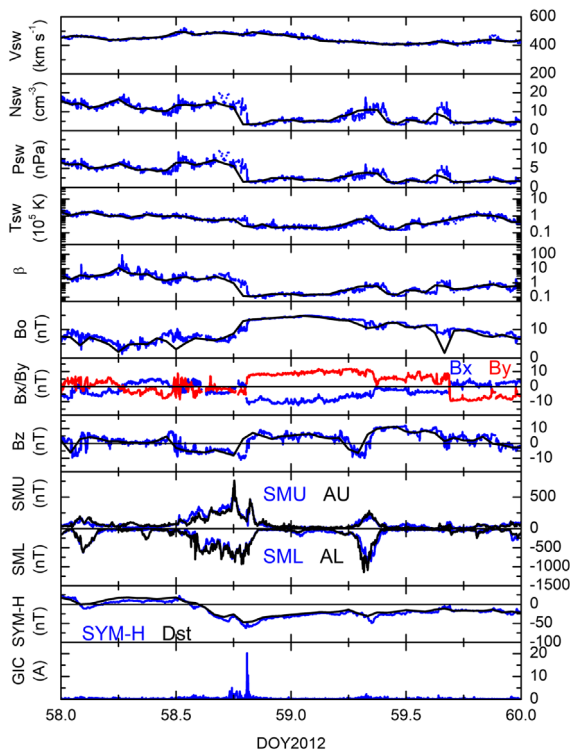


Fig. A38. Events on day 58 (27 February) 2012. Same format as in Figure A1.

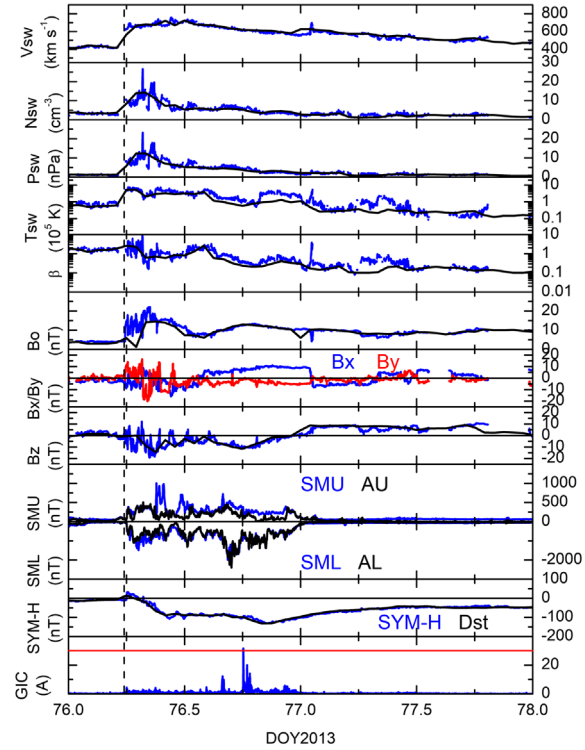


Fig. A40. Events on day 76 (17 March) 2013. Same format as in Figure A1. The horizontal red line indicates the GIC = 30 A level.

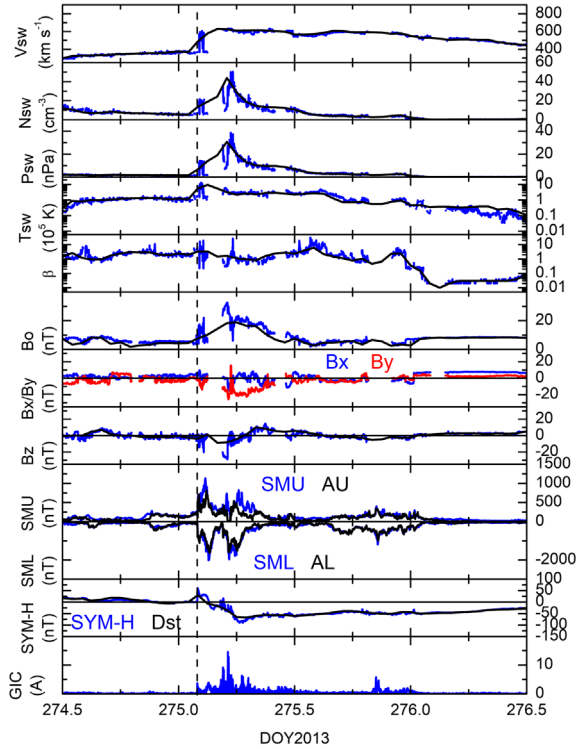


Fig. A41. Events on day 275 (2 October) 2013. Same format as in Figure A1.

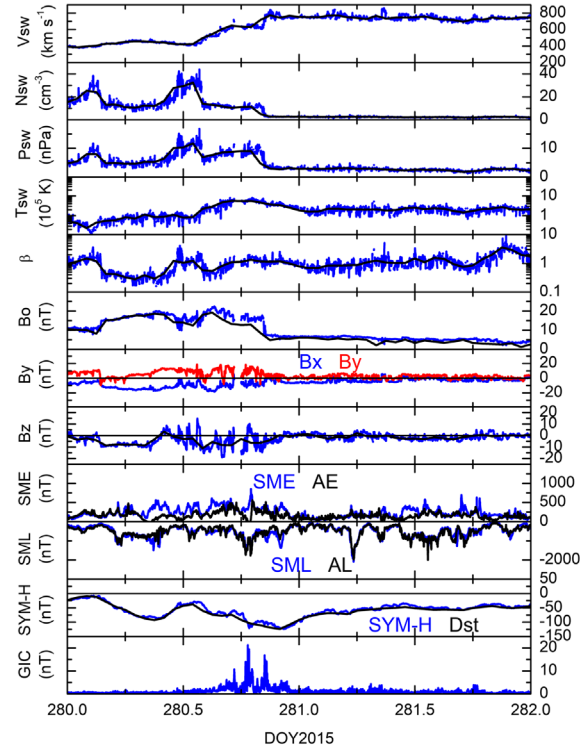


Fig. A43. Events on day 280 (7 October) 2015. Same format as in Figure A1.

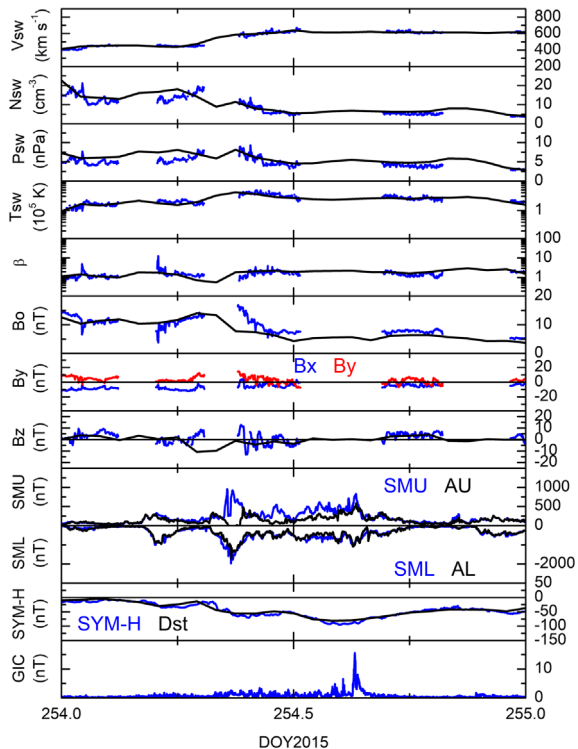


Fig. A42. Events on day 254 (11 September) 2015. Same format as in Figure A1.

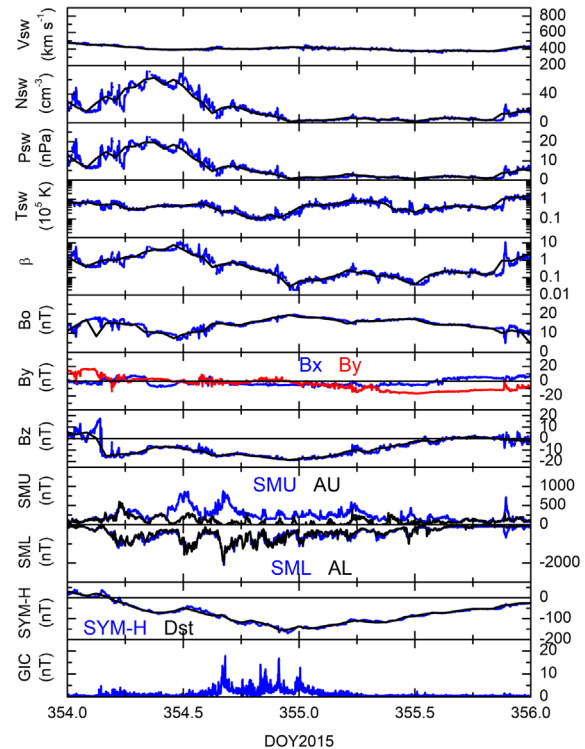


Fig. A44. Events on day 354 (20 December) 2015. Same format as in Figure A1.

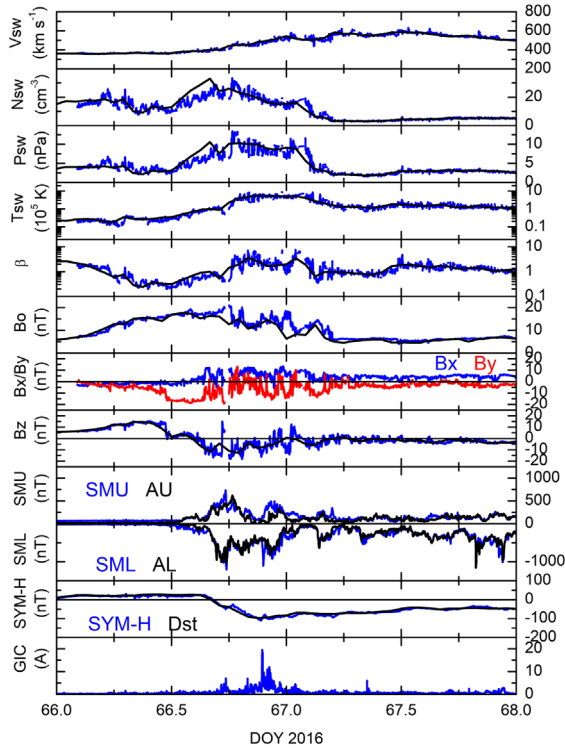


Fig. A45. Events on day 66 (6 March) 2016. Same format as in Figure A1.

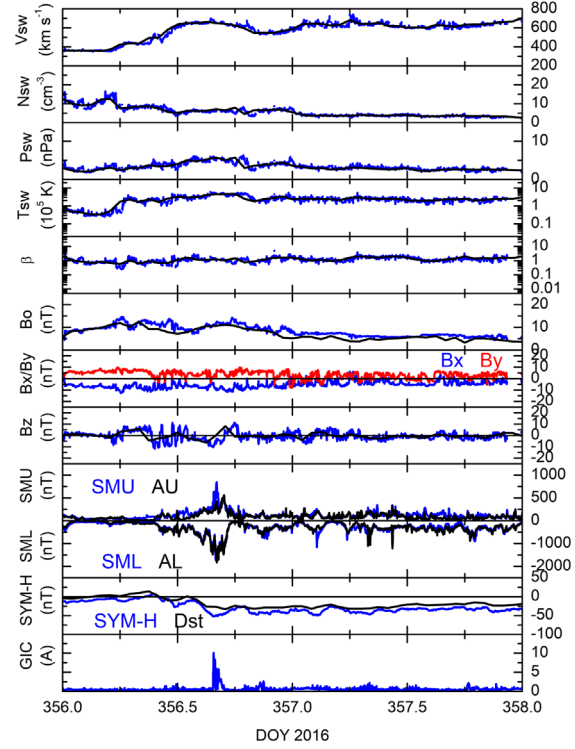


Fig. A47. Events on day 356 (21 December) 2016. Same format as in Figure A1.

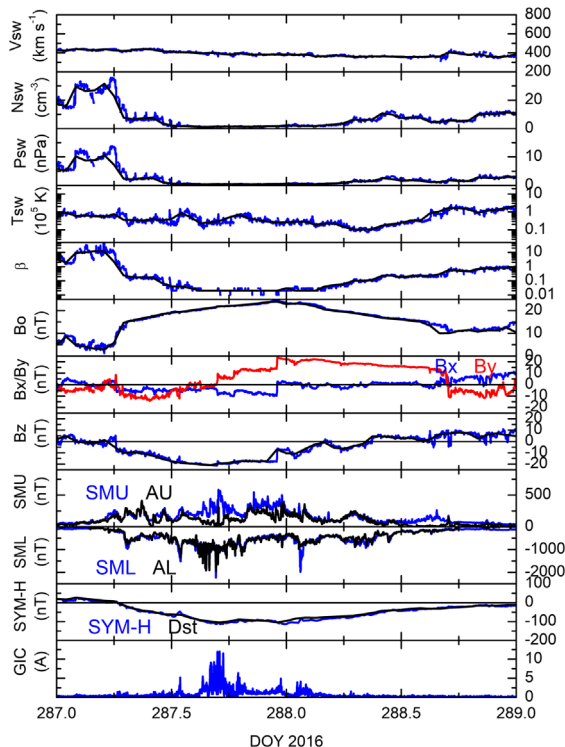


Fig. A46. Events on day 287 (13 October) 2016. Same format as in Figure A1.

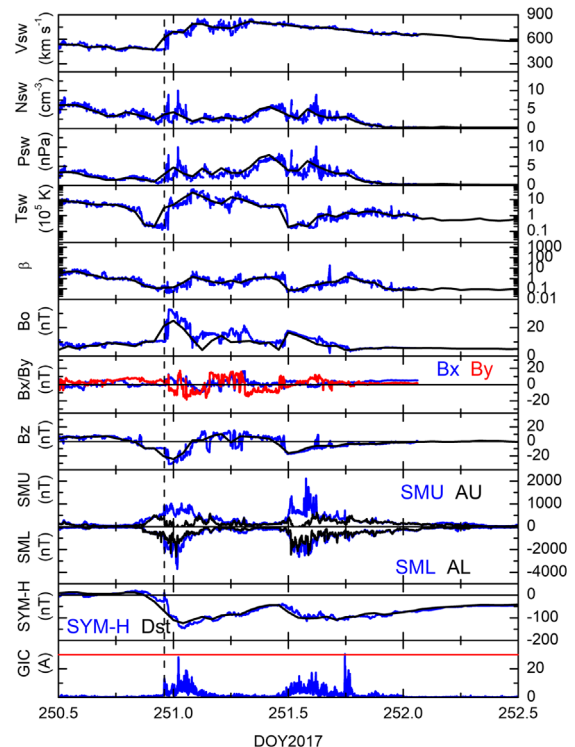


Fig. A48. Events on day 251 (8 September) 2017. Same format as in Figure A1. The horizontal red line indicates the GIC = 30 A level.

any obvious substorm spike. It was associated with an IMF Bs-to-Bn turning at a solar wind ram pressure decrease caused by a fast reverse shock.

Day 354 (20 December), 2015 (Fig. A44). A slow $V_{sw} \sim 430 \text{ km s}^{-1}$ ICME MC event. Pileup region Bs and MC Bs created a double dip storm with $SYM-H = -77 \text{ nT}$ and -170 nT intensities. The pileup region Bs created the first storm dip and the slow MC Bs the second dip. There is no shock. There are no intense GICs in the first dip storm. Although the MC contains a constant Bs field here is a lot of auroral (SML) activity throughout the second dip storm. A double peak GIC of 14 and 18 A intensities is associated with an intense substorm of $SML = -2106 \text{ nT}$. There are 3 more GIC clusters of smaller intensities with peak GICs $> 10 \text{ A}$ that appear to be associated with smaller amplitude substorms.

Day 66 (6 March), 2016 (Fig. A45). A slow speed stream/HSS ($V_{sw} \sim 590 \text{ km s}^{-1}$) interaction created a CIR, and the Bs in the CIR caused a $SYM-H = -110 \text{ nT}$ storm. There was no shock. Within the CIR are Bz fluctuations superposed on a constant Bs biased interval, the latter of which caused the storm main phase. There is large geomagnetic activity up to $SML = -1207 \text{ nT}$ but no associated GICs above study threshold. A 20 A GIC event was caused by a $SML = -1105 \text{ nT}$ short duration substorm. This SME spike was not detected in the AL index. This GIC occurred at storm maximum.

Day 287 (Oct 13), 2016 (Fig. A46). A low speed MC of $V_{sw} \sim 410 \text{ km s}^{-1}$ with peak magnetic field magnitude of $\sim 24 \text{ nT}$ and peak Bs of $\sim 21 \text{ nT}$ caused a $SYM-H = -114 \text{ nT}$

magnetic storm. There is a large cluster of GICs with peak values reaching 12 A occurring near the storm peak. The GICs were associated with large substorms which have a peak intensity of $SML = -2230 \text{ nT}$. One substorm of $SML = -1323 \text{ nT}$ intensity is correlated with a GIC spike of 12 A intensity.

Day 356 (21 December), 2016 (Fig. A47). A $V_{sw} \sim 650 \text{ km s}^{-1}$ HSS Bs created a weak magnetic storm of $SYM-H = -52 \text{ nT}$. A small long duration Bs (with oscillations) caused a cluster of high frequency substorms with a delayed peak intensity of $SML = -1721 \text{ nT}$. The peak of the substorm is associated with a $\sim 10 \text{ A}$ GIC cluster. In the cluster there is one event with magnitude greater than 10 A.

Days 251 (8 September), 2017 (Fig. A48). A double dip magnetic storm of $SYM-H = -146 \text{ nT}$ and -115 nT were generated by the upstream shock/sheath Bs and the trailing MC Bs, respectively. The shock compresses pre-existing Bs leading to a storm of -146 nT . The shock at $\sim 2303 \text{ UT}$ (0203 LT) causes a GIC below the study threshold. At the time of the shock Mäntsälä was in the midnight-dawn sector. A cluster of substorms occurred in the first storm main phase. A maximum intensity GIC of 28 A is correlated with a short duration $SML = -3712 \text{ nT}$ supersubstorm. There is a cluster of intense substorms/SSSs with amplitudes up to $SML = -2511 \text{ nT}$ and GICs up to 18 A intensity associated with the second storm main phase. There are no obvious 1-to-1 relationships between GIC events and substorms. The largest GIC of this interval occurred in the storm recovery phase, had an intensity of 30 A and cannot be associated with any large substorm or any solar wind feature.

Cite this article as: Tsurutani BT & Hajra R 2021. The Interplanetary and Magnetospheric causes of Geomagnetically Induced Currents (GICs) $> 10 \text{ A}$ in the Mäntsälä Finland Pipeline: 1999 through 2019. *J. Space Weather Space Clim.* **11**, 23. <https://doi.org/10.1051/swsc/2021001>.